NASA CR-112252

A STUDY OF MODAL COUPLING PROCEDURES FOR THE SPACE SHUTTLE

By S. Goldenberg and M. Shapiro

Prepared under Contract No. NAS-10635-8 by
GRUMMAN AEROSPACE CORPORATION
Bethpage, New York 11714

for

NATIONAL AERONAUTICS AND SPACE ADMINISTRATION

FOREWORD

This report is submitted to the NASA Langley Research Center in partial fulfillment of Master Agreement Contract NAS-10635-8. This contract involves the formulation, evaluation, and demonstration of various procedures for analytically coupling two or more substructures to obtain modal data for the assembly, using data obtained from mode surveys of the individual components.

Dr. Robert W. Fralich of the NASA Langley Research Center is the Technical Monitor. Mr. Eugene F. Baird of the Grumman Aerospace Corporation is the Master Agreement Program Manager, and Mr. Stephen Goldenberg of Grumman is the Project Manager.

TABLE OF CONTENTS

SUMMARY	1
INTRODUCTION	3
SYMBOLS	5
FORMULATION OF COUPLING PROCEDURES	12
General Coupling Procedure	14
Free Junction Points	23
Mass Loaded Junction Points	25
Fixed Junction Points	27
Fixed Base	34
ANALYTICAL VERIFICATION	35
Orbiter/Tank Coupling	35
Orbiter/Booster Coupling	40
EXPERIMENTAL VERIFICATION	45
CONCLUSIONS AND RECOMMENDATIONS	48
APPENDIX - CALCULATION OF INTERNAL DISPLACEMENTS DUE TO UNIT JUNCTION POINT MOTIONS USING MODE SURVEY DATA	50
REFERENCES	53
TABLES	54
FIGURES	62

SUMMARY

The purpose of this study was to formulate, evaluate, and demonstrate various procedures for analytically coupling two or more substructures to obtain modal data for the assembly, using data obtained from mode surveys of the individual components. Particular attention was paid to the applicability of the techniques investigated to the Space Shuttle, with the possible replacement of full scale mode surveys of the shuttle assembly by component mode surveys along with analytical coupling.

The synthesis procedures formulated in this report can all handle redundant connections, although the presence of redundancies does add complication to one of the techniques. All of the procedures use the test data directly, without going through an intermediate analytical model, and no analytical stiffness data is required to supplement the mode survey data.

The coupling procedures were initially verified and evaluated by applying them to analytical check problems. Lumped parameter analysis was used to compute the modal properties of an assembly and its components. The analytical component modes were then coupled, and the results compared with those obtained by direct analysis of the assembly. The two most promising procedures, determined from the accuracy of the results and from the ease of obtaining the required experimental data, were then applied to test data.

Experimental data were obtained for a 1/15 scale dynamic model of an early space shuttle configuration, which consisted of an orbiter and a booster. Mode surveys were performed on the orbiter, booster, and coupled orbiter/booster. The orbiter, and booster data were then synthesized, and the results compared with those obtained from direct test of the assembly.

Results presented in this report show that the modes of an assembly can indeed be successfully synthesized from mode survey data for the individual

components. Of the techniques studied, the most promising for shuttle application involves the use of component modes which are obtained with known weights attached to the junction points. This procedure, known as mass loading, provides the least complicated means of "working" or deforming the local structure near interface boundaries in the lower component modes. Mass loading improves convergence of the synthesis procedure for assembly modes having significant local structure deformation by lowering the frequencies of the modes in which the local structure is deformed, and thus reducing the total number of component modes required for coupling. Just how much advantage is gained through the use of mass loading is, however, highly dependent on the nature of the structure.

INTRODUCTION

The dynamic characteristics of aerospace structures, as represented by their normal modes of vibration, are required for many purposes, including aeroelastic analysis, calculation of structural response to dynamic loadings, and control system analysis to name a few. In the design stage modal data is customarily obtained from a lumped parameter analysis. When hardware becomes available, mode surveys are performed to provide experimental verification of the analytical data. Because of its size, full-scale vibration testing of an entire space shuttle assembly is a very large and costly task, which may require the construction of a new facility to accommodate it. For this reason an alternate approach to this problem, modal coupling, is being considered. The use of modal coupling which is the subject of this investigation would permit the limitation of vibration testing to components. Assembly modes would then be analytically synthesized from the component mode survey data. Furthermore, since modal data for the individual components are required in any event, a reduction in the total amount of testing could be affected in addition to avoiding the costly assembly test.

A great deal of work has been done in the field of modal coupling using data obtained from analysis of the components. The objective of this work has been to reduce the size of the eigenvalue problem which must be solved for problems having a large number of degrees of freedom. This is accomplished by breaking the structure into a number of substructures, solving the eigenvalue problem for each substructure, and using only the lower component modes in the coupling. Since they were developed for use with an analytical model of the structure, most of these procedures require data, in addition to modal prcperties, which are not readily available from a test. These additional data include stiffness matrices, and static deflection shapes. More recently, work has been directed towards making use of modal data obtained from vibration testing rather than analysis.

Coupling procedures are formulated in this report which require only data which are readily available from substructure testing. These procedures are basically existing techniques which have been adapted to suit the purposes of this study. They are first applied to two analytical check problems in order to verify and evaluate them without introducing the uncertainties associated with test data. The coupling procedures are then applied to test data for a NASA Langley Research Center (LRC) 1/15 scale model of a space shuttle configuration. The mode surveys were performed by Mr. Robert Herr of NASA/LRC, and the data were processed by the Systems Group of TRW at Redondo Beach. The authors also wish to acknowledge the contributions of Mr. Robert Goldstein, who did much of the coding and computations at Grumman, and Mr. Edwin Lerner of Grumman, who made significant contributions to the coupling procedures contained in this report.

SYMBOLS

$[\ ]$	Matrix
$\lceil \ \rfloor$	Diagonal matrix
$[\ ]^T$	Transpose of a matrix
$[\ ]^{-1}$	Inverse of a matrix
$\{\ \}$	Column vector
$\{\ \}^T$	Row vector
$\{\dot{\ }\}$	First time derivative of a vector
$\{\ddot{\ }\}$	Second time derivative of a vector
$[C_x]$	Damping matrix for the uncoupled substructures in the physical or "x" coordinate system
$[C_{x_i}]$	Damping matrix for the i^{TH} substructure in the physical or "x" coordinate system (a submatrix of $[C_x]$)
$[C_\eta]$	Damping matrix in the "coupled system modal" or "η" coordinate system
$[C_\xi]$	Damping matrix for the uncoupled substructures in the component modal or "ξ" coordinate system
$[C_{\xi_i}]$	Damping matrix for the i^{TH} substructure in the component modal or "ξ" coordinate system (a submatrix of $[C_\xi]$)

$[C_{\hat{\xi}}]$ Damping matrix in the "coupled component modal" or "$\hat{\xi}$" coordinate system

$\{F_J\}$ Vector of junction point forces in the physical or "x" coordinate system

$\{F_x\}$ Vector of forces on the uncoupled substructures in the physical or "x" coordinate system

$\{F_{x_i}\}$ Vector of forces on the i^{TH} substructure in the "x" or physical coordinate system

$\{F^I_{x_i}\}$ Vector of internal point forces on the i^{TH} substructure in the "x" or physical coordinate system

$\{F^J_{x_i}\}$ Vector of junction point forces on the i^{TH} substructure in the "x" or physical coordinate system

$\{F_\eta\}$ Vector of forces in the "coupled system modal" or "η" coordinate system

$\{F_\xi\}$ Vector of forces on the uncoupled substructures in the component modal or "ξ" coordinate system

$\{F_{\xi_i}\}$ Vector of forces on the i^{TH} substructure in the component modal or "ξ" coordinate system

$\{F_{\hat{\xi}}\}$ Vector of applied forces in the "coupled component modal" or "$\hat{\xi}$" coordinate system

$[I]$ Identity matrix

$[K_x]$, $[M_x]$ Stiffness and mass matrices for the uncoupled substructures in the physical or "x" coordinate system

$[K_{x_i}]$, $[M_{x_i}]$ Stiffness and mass matrices for the i^{TH} substructure in the physical or "x" coordinate system (submatrices of $[K_x]$ and $[M_x]$)

$[K_\eta]$, $[M_\eta]$ Stiffness and mass matrices in the "coupled system modal" or "η" coordinate system

$[K_\xi]$, $[M_\xi]$ Stiffness and mass matrices for the uncoupled substructure in the component modal or "ξ" coordinate system

$[K_\xi^{jk}]$, $[M_\xi^{jk}]$ Submatrices of component modal stiffness and mass matrices (jk is a general index which takes on specific symbols defined in the list of superscripts)

$[K_\xi']$, $[M_\xi']$ Stiffness and mass matrices for a substructure in the component modal or "ξ" coordinate system (obtained using fixed junction normal modes and junction point displacements)

$[K_\xi^*]$, $[M_\xi^*]$ Stiffness and mass matrices for a substructure in the component modal or "ξ" coordinate system (obtained using fixed junction normal modes, rigid body modes, and constraint modes)

$[K_{\xi_i}]$, $[M_{\xi_i}]$ Stiffness and mass matrices for the i^{TH} substructure in the component modal or "ξ" coordinate system (submatrices of $[K_\xi]$ and $[M_\xi]$)

$[K_{\xi_i}^k]$, $[M_{\xi_i}^k]$ Submatrices of component modal stiffness and mass matrices (k is a general index which takes on specific symbols defined in the list of superscripts)

$\left[K_{\hat{\xi}}\right]$, $\left[M_{\hat{\xi}}\right]$ Stiffness and mass matrices in the "coupled component modal" or "$\hat{\xi}$" coordinate system

$\left[M_x^L\right]$ Mass matrix of the added masses used for mass loading in the physical or "x" coordinate system

$\left[M_x^S\right]$ Component mass matrix excluding mass loading in the physical or "x" coordinate system

$\left[M_\xi^S\right]$ Component mass matrix excluding mass loading in the component modal or "ξ" coordinate system.

$\left[M_{\hat{\xi}}^S\right]$ Mass matrix excluding mass loading in the coupled component modal or "$\hat{\xi}$" coordinate system

$[T]$ Transformation matrix between the "ξ" and "$\hat{\xi}$" coordinate systems

$\{x\}$ Vector of uncoupled substructure absolute displacements in the physical or "x" coordinate system

$\{x^I\}$ Vector of component internal point absolute displacements in the physical or "x" coordinate system

$\{x^J\}$ Vector of component junction point absolute displacements in the physical or "x" coordinate system

$\{\overset{=}{x}\}$ Vector of component physical displacements relative to the junction points

$\{\tilde{x}\}$ Vector of component physical displacements due to junction point motion

$\{\overset{=I}{x}\}$ Vector of component internal physical displacements relative to the junction points

$\{\tilde{x}^I\}$ Vector of component internal physical displacements due to junction point motion

$\{x_i\}$ Vector of absolute displacements for the i^{TH} substructure in the physical or "x" coordinate system

$\{x_i^I\}$ Vector of internal point absolute displacements for the i^{TH} substructure in the physical or "x" coordinate system

$\{x_i^J\}$ Vector of junction point displacements for the i^{TH} substructure in the physical or "x" coordinate system

$\{\eta\}$ Vector of coupled system modal displacements

$\{\xi\}$ Vector of uncoupled component modal displacements

$\{\xi_i\}$ Vector of component modal displacements for the i^{TH} substructure

$\{\xi^C\}$ Vector of component modal displacements associated with constraint modes

$\{\xi^N\}$ Vector of component modal displacements associated with normal modes

$\{\xi^R\}$ Vector of component modal displacements associated with rigid body modes

$\{\hat{\xi}\}$ Vector of coupled component modal displacements

$\{\xi'\}$ Vector of component modal displacements made up of junction point displacements and the generalized displacements associated with fixed junction normal modes

$\{\xi^*\}$ Vector of component modal displacements made up of the generalized displacements associated with fixed base normal modes, rigid body modes, and constraint modes

$[\sigma]$ Matrix giving internal point displacements due to junction point motion in the physical or "x" coordinate system

$\left[\varphi_I^C\right]$ Submatrix of the component mode shape matrix giving internal displacements associated with constraint modes

$\left[\varphi_I^N\right]$ Submatrix of the component mode shape matrix giving internal displacements associated with normal modes

$\left[\varphi_I^R\right]$ Submatrix of the component mode shape matrix giving internal displacements associated with rigid body modes

$\left[\varphi_J^C\right]$ Submatrix of the component mode shape matrix giving junction point displacements associated with constraint modes

$\left[\varphi_J^R\right]$ Submatrix of the component mode shape matrix giving junction point displacements associated with rigid body modes

$[\varphi_x]$ Matrix of uncoupled component mode shapes

$[\varphi_x']$ Matrix of component mode shapes made up of fixed junction normal modes and unit junction displacements

$[\varphi_x^*]$ Matrix of component mode shapes made up of fixed junction normal modes, rigid body modes, and constraint modes

$\left[\varphi_{x_i}\right]$ Matrix of component mode shapes for the i^{TH} substructure (a submatrix of $\left[\varphi_x\right]$)

$\left[\varphi^I_{x_i}\right]$ Submatrix of $\left[\varphi_{x_i}\right]$ containing only internal point displacements

$\left[\varphi^J_{x_i}\right]$ Submatrix of $\left[\varphi_{x_i}\right]$ containing only junction point displacements

$\left[\varphi^N_{x_i}\right]$ Submatrix of $\left[\varphi_{x_i}\right]$ containing only normal modes

$\left[\varphi^R_{x_i}\right]$ Submatrix of $\left[\varphi_{x_i}\right]$ containing only rigid body modes

$\left[\varphi_x\right]$ Matrix of assembly mode shapes in the physical or "x" coordinate system

$\left[\varphi_{\hat{\xi}}\right]$ Matrix of assembly mode shapes in the coupled component modal or "$\hat{\xi}$" coordinate system

$\omega_{\hat{\xi}}$ Circular frequency of the assembly

$\left[\omega^2_i\right]$ Diagonal matrix whose elements are the circular frequencies squared of the i^{TH} substructure

Superscripts:

C	Constraint Modes
J	Junction Point Displacements
N	Normal Modes
R	Rigid Body Modes

FORMULATION OF COUPLING PROCEDURES

Procedures will now be formulated for analytically coupling two or more substructures to obtain modal data for the assembly using data from mode surveys of the individual components. In order to perform the synthesis, the mode shapes, modal mass, and modal stiffnesses of each component must be known. Although damping is discussed briefly, Reference 1 should be consulted for a complete discussion of the damping synthesis portion of this study. All of the data required by the synthesis procedures other than the mass properties are readily available from substructure testing and rigid body considerations. No elastic analysis is required.

The component modal mass and stiffness matrices are coupled by requiring junction point compatibility. Solution of the eigenvalue problem associated with these mass and stiffness matrices yields the undamped modal properties of the assembly. The modal damping matrix for the assembly is obtained from the component modal damping matrices by using the transformations developed for the undamped problem. The only approximation introduced in the synthesis is due to representing the components by only their lower modes of vibration. A sufficient number of component modes must be employed to establish junction point compatibility, and to represent the deformations of the coupled substructures. The number of modes required depends on the type of component modes employed as well as the nature of the structure.

A general coupling procedure based on the work of Hurty (Reference 2) is first formulated. Although Hurty's work deals only with fixed junction point component modes, the procedure developed here makes no restriction on the type of component modes employed. Specific procedures are then discussed. They differ only in the type of component modes employed, i.e., in the boundary conditions used in the component mode survey. The first of these deals with free junction point modes, and although this case was treated by Hou (Reference 3), it can be seen that it is just a special case of the general coupling procedure, and differs analytically from Hurty's method only in

that no constraint modes are required. The use of mass loaded junction points, which was suggested by the interface inertia loading of Reference 4 is discussed next. The procedure developed here is, however, quite different, from that of Reference 4, since it is intended to make use of experimental rather than analytical data for the components. Next, the use of fixed junction point component modes is treated. Although the development is initially along the lines of Reference 5 because the physical significance is clearer, the final formulation is that of Hurty (Reference 2) which reduces the testing required. The application of this method to test data required the development of additional techniques for the determination of the constraint modes and the associated stiffness terms. Finally, fixed base component modes are treated. It is seen that the formulation for fixed base component modes does not differ from that for fixed junction point component modes.

It should be noted that the general coupling procedure may be employed to synthesize component modal data obtained with any combination of support conditions on the various substructures, e.g., a free-free structure may be coupled with one having fixed or mass loaded junction points.

Although the formulation is developed for two substructures, any number of components may be coupled through repeated application. To couple substructures "a", "b", and "c", one would first couple "a" and "b" to obtain modal data for the subassembly "a/b", and then couple "a/b" with "c". Since the intermediate results for the subassembly are quite often useful it does not pay to couple all components at once, although the formulation could be easily extended to do this.

General Coupling Procedure

The equations of motion for the uncoupled substructures "a" and "b" may be written in the "physical" or "x" coordinate system, as

$$\left[M_x\right]\left\{\ddot{x}\right\} + \left[C_x\right]\left\{\dot{x}\right\} + \left[K_x\right]\left\{x\right\} = \left\{F_x\right\} \tag{1a}$$

where $\left[M_x\right]$, $\left[C_x\right]$, and $\left[K_x\right]$ are the mass, damping, and stiffness matrices, and $\left\{F_x\right\}$ is the vector of applied forces, in partitioned form:

$$\left[\begin{array}{c:c} M_{x_a} & \\ \hdashline & M_{x_b} \end{array}\right] \left\{\begin{array}{c} \ddot{x}_a \\ \hdashline \ddot{x}_b \end{array}\right\} + \left[\begin{array}{c:c} C_{x_a} & \\ \hdashline & C_{x_b} \end{array}\right] \left\{\begin{array}{c} \dot{x}_a \\ \hdashline \dot{x}_b \end{array}\right\} + \left[\begin{array}{c:c} K_{x_a} & \\ \hdashline & K_{x_b} \end{array}\right] \left\{\begin{array}{c} x_a \\ \hdashline x_b \end{array}\right\} = \left\{\begin{array}{c} F_{x_a} \\ \hdashline F_{x_b} \end{array}\right\} \tag{1b}$$

Here the subscripts "a" and "b" designate substructures "a" and "b", respectively, and the $\{x\}$'s may include rotations as well as displacements.

Equations (1) may be transformed into the "uncoupled component modal" or "ξ" coordinate system, which is defined by

$$\{x\} = \left[\varphi_x\right]\{\xi\} \tag{2a}$$

or

$$\left\{\begin{array}{c} x_a \\ \hdashline x_b \end{array}\right\} = \left[\begin{array}{c:c} \varphi_{x_a} & \\ \hdashline & \varphi_{x_b} \end{array}\right] \left\{\begin{array}{c} \xi_a \\ \hdashline \xi_b \end{array}\right\} \tag{2b}$$

where the columns of $[\varphi_x]$ are component mode shapes. The types of mode shapes included in this matrix depend on the support conditions used in the component tests, and will be fully discussed, along with the testing required to determine them, in the next four sections.

Substituting equations (2) into equations (1), and premultiplying by $[\varphi_x]^T$ gives

$$[M_\xi]\{\ddot{\xi}\} + [C_\xi]\{\dot{\xi}\} + [K_\xi]\{\xi\} = \{F_\xi\} \tag{3a}$$

or

$$\left[\begin{array}{c|c} M_{\xi_a} & \\ \hline & M_{\xi_b} \end{array}\right]\left\{\begin{array}{c} \ddot{\xi}_a \\ \hline \ddot{\xi}_b \end{array}\right\} + \left[\begin{array}{c|c} C_{\xi_a} & \\ \hline & C_{\xi_b} \end{array}\right]\left\{\begin{array}{c} \dot{\xi}_a \\ \hline \dot{\xi}_b \end{array}\right\} + \left[\begin{array}{c|c} K_{\xi_a} & \\ \hline & K_{\xi_b} \end{array}\right]\left\{\begin{array}{c} \xi_a \\ \hline \xi_b \end{array}\right\} = \left\{\begin{array}{c} F_{\xi_a} \\ \hline F_{\xi_b} \end{array}\right\} \tag{3b}$$

where

$$[M_\xi] = [\varphi_x]^T [M_x] [\varphi_x] \quad \ldots \text{ uncoupled modal mass matrix} \tag{3c}$$

$$[C_\xi] = [\varphi_x]^T [C_x] [\varphi_x] \quad \ldots \text{ uncoupled modal damping matrix} \tag{3d}$$

$$[K_\xi] = [\varphi_x]^T [K_x] [\varphi_x] \quad \ldots \text{ uncoupled modal stiffness matrix} \tag{3e}$$

$$\{F_\xi\} = [\varphi_x]^T \{F_x\} \quad \ldots \text{ uncoupled modal force vector} \tag{3f}$$

$$\left.\begin{array}{l} [M_{\xi_a}] = [\varphi_{x_a}]^T [M_{x_a}] [\varphi_{x_a}] \\ [M_{\xi_b}] = [\varphi_{x_b}]^T [M_{x_b}] [\varphi_{x_b}] \end{array}\right\} \quad \ldots \text{ component modal mass matrices} \tag{3g, 3h}$$

$$\left[C_{\xi_a}\right] = \left[\varphi_{x_a}\right]^T \left[C_{x_a}\right] \left[\varphi_{x_a}\right] \tag{3i}$$

$$\left[C_{\xi_b}\right] = \left[\varphi_{x_b}\right]^T \left[C_{x_b}\right] \left[\varphi_{x_b}\right] \tag{3j}$$

... component modal damping matrices

$$\left[K_{\xi_a}\right] = \left[\varphi_{x_a}\right]^T \left[K_{x_a}\right] \left[\varphi_{x_a}\right] \tag{3k}$$

$$\left[K_{\xi_b}\right] = \left[\varphi_{x_b}\right]^T \left[K_{x_b}\right] \left[\varphi_{x_b}\right] \tag{3l}$$

... component modal stiffness matrices

$$\left\{F_{\xi_a}\right\} = \left[\varphi_{x_a}\right]^T \left\{F_{x_a}\right\} \tag{3m}$$

$$\left\{F_{\xi_b}\right\} = \left[\varphi_{x_b}\right]^T \left\{F_{x_b}\right\} \tag{3n}$$

... component modal force vectors

The component modal mass, damping, and stiffness matrices will be the input to the synthesis analysis. Modal mass and stiffness matrices are discussed in the next four sections, while component modal damping matrices are discussed in Reference 1.

Equation (3a) will now be transformed into the "coupled component modal" or "$\hat{\xi}$" coordinate system by constraining the junction points of the substructures to move together. First, Equation (2b) is rewritten in a partitioned form as

$$\left\{\begin{array}{c} x_a^I \\ \hline x_a^J \\ \hline\hline x_b^I \\ \hline x_b^J \end{array}\right\} = \left[\begin{array}{c|c} \varphi_{x_a}^I & \\ \hline \varphi_{x_a}^J & \\ \hline\hline & \varphi_{x_b}^I \\ \hline & \varphi_{x_b}^J \end{array}\right] \left\{\begin{array}{c} \xi_a \\ \hline\hline \xi_b \end{array}\right\} \tag{4}$$

where the superscripts "I" and "J" refer to internal and junction points, respectively. Junction points are those points at which the two components are attached, while internal points are the remaining points. Component mode shapes must include all junction point displacement. The compatibility relationship for junction point displacements may be written as

$$\left\{x_a^J\right\} - \left\{x_b^J\right\} = 0 \tag{5a}$$

or, making use of Equation (4),

$$\left[\varphi_{x_a}^J \;\vdots\; -\varphi_{x_b}^J\right] \left\{\begin{array}{c} \xi_a \\ \hline \xi_b \end{array}\right\} = \{0\} \tag{5b}$$

or

$$\left[\varphi_J\right]\{\xi\} = \{0\} \tag{5c}$$

Next, Equation (5c) is arbitrarily partitioned

$$\left[\bar{\varphi}_J \,\vdots\, \hat{\varphi}_J\right] \left\{\begin{matrix}\bar{\xi} \\ \hat{\xi}\end{matrix}\right\} = \{0\} \tag{5d}$$

where $\left[\bar{\varphi}_J\right]$ is a nonsingular-square partition of $\left[\varphi_J\right]$, and $\left[\hat{\varphi}_J\right]$ is the remaining partition. It should be noted that this requires that the number of component modes be greater than the number of junction point displacements. Solving Equation (5d) for $\{\bar{\xi}\}$ gives

$$\{\bar{\xi}\} = -\left[\bar{\varphi}_J\right]^{-1}\left[\hat{\varphi}_J\right]\{\hat{\xi}\} \tag{5e}$$

and the transformation from the $\{\xi\}$ to the $\{\hat{\xi}\}$ coordinate system is

$$\left\{\begin{matrix}\bar{\xi} \\ \hat{\xi}\end{matrix}\right\} = \left[\begin{matrix}-\bar{\varphi}_J^{-1}\hat{\varphi}_J \\ I\end{matrix}\right]\left\{\hat{\xi}\right\} \tag{6a}$$

or

$$\{\xi\} = [T]\{\hat{\xi}\} \tag{6b}$$

Substituting Equation (6b) into Equation (3a), and premultiplying by $[T]^T$ yields

$$\left[M_{\hat{\xi}}\right]\left\{\ddot{\hat{\xi}}\right\} + \left[C_{\hat{\xi}}\right]\left\{\dot{\hat{\xi}}\right\} + \left[K_{\hat{\xi}}\right]\left\{\hat{\xi}\right\} = \left\{F_{\hat{\xi}}\right\} \tag{7a}$$

where

$$\left[M_{\hat{\xi}}\right] = \left[T\right]^T \left[M_\xi\right] \left[T\right] \tag{7b}$$

$$\left[C_{\hat{\xi}}\right] = \left[T\right]^T \left[C_\xi\right] \left[T\right] \tag{7c}$$

$$\left[K_{\hat{\xi}}\right] = \left[T\right]^T \left[K_\xi\right] \left[T\right] \tag{7d}$$

$$\left\{F_{\hat{\xi}}\right\} = \left[T\right]^T \left\{F_\xi\right\} \tag{7e}$$

The right hand side of Equation (7a) will now be examined. We first partition Equation (3f):

$$\left\{\begin{array}{c} F_{\xi_a} \\ \hline F_{\xi_b} \end{array}\right\} = \left[\begin{array}{c|c|c|c} \varphi_{x_a}^{I\,T} & \varphi_{x_a}^{J\,T} & & \\ \hline & & \varphi_{x_b}^{I\,T} & \varphi_{x_b}^{J\,T} \end{array}\right] \left\{\begin{array}{c} F_{x_a}^I \\ \hline F_{x_a}^J \\ \hline F_{x_b}^I \\ \hline F_{x_b}^J \end{array}\right\} \tag{8}$$

where the meanings of the subscripts and superscripts are the same as in Equation (4). For free vibration of the coupled system, the only forces on the substructures are the equal and opposite forces at the junction points. Thus,

$$\left\{ F^{I}_{x_a} \right\} = \left\{ F^{I}_{x_b} \right\} = \{ 0 \} \tag{9a}$$

and

$$\left\{ F^{J}_{x_a} \right\} = \left\{ - F^{J}_{x_b} \right\} \equiv \left\{ F_J \right\} \tag{9b}$$

combining Equations (8), (9a), and (9b) gives

$$\begin{Bmatrix} F_{\xi_a} \\ - - - \\ F_{\xi_b} \end{Bmatrix} = \begin{bmatrix} \varphi^{T}_{J x_a} \\ - - - \\ - \varphi^{T}_{J x_b} \end{bmatrix} \left\{ F_J \right\} \tag{10a}$$

or

$$\{ F_{\xi} \} = [\varphi_J]^{T} \{ F_J \} \tag{10b}$$

and, substituting this into Equation (7e),

$$\{ F_{\hat{\xi}} \} = [T]^{T} [\varphi_J]^{T} \{ F_J \} \tag{11a}$$

or

$$\left\{F_{\hat{\xi}}\right\} = \left[\begin{array}{cc:c} -\hat{\varphi}_J^T & \bar{\varphi}_J^{-T} & I \end{array}\right]\left[\begin{array}{c} \bar{\varphi}_J^T \\ \hline -\hat{\varphi}_J^T \end{array}\right]\left\{F_J\right\} = [0]\left\{F_J\right\} \tag{11b}$$

therefore

$$\left\{F_{\hat{\xi}}\right\} = \{0\} \tag{11c}$$

The free vibration equations for the assembly are from Equations (7a) and (11c),

$$\left[M_{\hat{\xi}}\right]\left\{\ddot{\hat{\xi}}\right\} + \left[C_{\hat{\xi}}\right]\left\{\dot{\hat{\xi}}\right\} + \left[K_{\hat{\xi}}\right]\left\{\hat{\xi}\right\} = \{0\} \tag{12}$$

and the undamped eigenvalue problem is

$$\left[K_{\hat{\xi}}\right]\left\{\varphi_{\hat{\xi}}\right\} = \omega_{\hat{\xi}}^2\left[M_{\hat{\xi}}\right]\left\{\varphi_{\hat{\xi}}\right\} \tag{13}$$

The solution of Equation (13) yields the circular frequencies, the $\omega_{\hat{\xi}}$'s, and mode shapes, the $\left\{\varphi_{\hat{\xi}}\right\}$'s, of the coupled system. These mode shapes, however, are in the "$\hat{\xi}$" coordinate system, and must be transformed to the "physical" coordinate system. From Equations (2a) and (6b)

$$\left[\varphi_x\right] = \left[\varphi_x\right]\left[T\right]\left[\varphi_{\hat{\xi}}\right] \tag{14}$$

where $\left[\varphi_{\underline{x}}\right]$ is the matrix of mode shapes of the assembly in the physical coordinate system, and $\left[\varphi_{\hat{\xi}}\right]$ is a matrix whose columns are the $\left\{\varphi_{\hat{\xi}}\right\}$'s.

Finally, for use with externally applied forces, Equation (7a) can be transformed into the "coupled system modal" coordinate system, "η", by leting

$$\left\{\hat{\xi}\right\} = \left[\varphi_{\hat{\xi}}\right]\left\{\eta\right\} \tag{15}$$

and premultiplying by $\left[\varphi_{\hat{\xi}}\right]^T$:

$$\left[M_\eta\right]\left\{\ddot{\eta}\right\} + \left[C_\eta\right]\left\{\dot{\eta}\right\} + \left[K_\eta\right]\left\{\eta\right\} = \left\{F_\eta\right\} \tag{16a}$$

where

$$\left[M_\eta\right] = \left[\varphi_{\hat{\xi}}\right]^T \left[M_{\hat{\xi}}\right]\left[\varphi_{\hat{\xi}}\right] \tag{16b}$$

$$\left[C_\eta\right] = \left[\varphi_{\hat{\xi}}\right]^T \left[C_{\hat{\xi}}\right]\left[\varphi_{\hat{\xi}}\right] \tag{16c}$$

$$\left[K_\eta\right] = \left[\varphi_{\hat{\xi}}\right]^T \left[K_{\hat{\xi}}\right]\left[\varphi_{\hat{\xi}}\right] \tag{16d}$$

$$\left\{F_\eta\right\} = \left[\varphi_{\hat{\xi}}\right]^T \left\{F_{\hat{\xi}}\right\} \tag{16e}$$

Free Junction Points

This is the simplest of all the coupling procedures from the standpoint of the component testing as well as the analytical synthesis. A standard free-free mode survey is performed on each substructure to determine its frequencies, and mode shapes. The instrumentation must include transducers at the junction points so that the mode shapes include all junction point motions which are to be made compatible with those of the adjacent sub-structure.

The matrix of component mode shapes includes both rigid body and normal modes. For substructure "i"

$$\left[\varphi_{x_i}\right] = \left[\varphi^{R}_{x_i} \,\vdots\, \varphi^{N}_{x_i}\right] \tag{17}$$

where the superscripts "R" and "N" designate the rigid body and normal structural modes, respectively. Normal mode shapes are measured in the mode survey, while the rigid body mode shapes may be easily written by the analyst.

The component modal mass matrix also consists of rigid body and normal structural mode partitions:

$$\left[M_{\xi_i}\right] = \left[\begin{array}{c:c} M^{R}_{\xi_i} & \\ \hdashline & M^{N}_{\xi_i} \end{array}\right] \tag{18}$$

where

$$\left[M^R_{\xi_i}\right] = \left[\varphi^R_{x_i}\right]^T \left[M_{x_i}\right]\left[\varphi^R_{x_i}\right]$$

$$\left[M^N_{\xi_i}\right] = \left[\varphi^N_{x_i}\right]^T \left[M_{x_i}\right]\left[\varphi^N_{x_i}\right]$$

Since $\left[K_{x_i}\right]$ is not known from test data, component modal stiffness matrices are computed from

$$\left[K_{\xi_i}\right] = \left[M_{\xi_i}\right]\left[\omega_i^2\right] \tag{19}$$

where $\left[\omega_i^2\right]$ is the diagonal matrix whose elements are the circular frequencies squared. In partitioned form

$$\left[K_{\xi_i}\right] = \left[\begin{array}{c|c} 0 & \\ \hline & K^N_{\xi_i} \end{array}\right] \tag{20}$$

Once these matrices have been obtained, the synthesis calculations are performed as shown in the previous section.

It should be noted that while free junction point synthesis is the most straight-forward procedure, it is by no means the best. The major shortcoming is that the local structure adjacent to the junction points is not "worked" in the lower component modes, and therefore the mode shapes obtained from the

component mode surveys do not contain local structure deformations. The lower modes of the assembly, on the other hand, will probably contain substantial local structure deformations due to the inertia loads imposed by the substructures on each other. This means that a relatively large number of substructure modes must be employed in the synthesis in order to include the modes which contain local structure motion.

Of course, the importance of the shortcoming just cited is highly dependent on the nature of the structure itself. If the substructures have very stiff local structure, then the assembly will not exhibit significant local structure motion in its lower modes, and the lack of local structure motion in the component modes will not be important. It is also possible for a substructure to have very flexible local structure and/or very heavy junction points. In this case, local structure motion would be reflected in the lower free-free component modes. Unfortunately, the situations hypothesized above, while they can and do occur, are not generally encountered.

Mass Loaded Junction Points

As discussed in the previous section, the shortcoming of free-free component modes is that the local structure is usually not worked in the lower modes. Through the use of "mass loading" this problem can be greatly reduced, with the addition of very little complication in the component testing and analytical synthesis.

When using mass loading, the component mode surveys are performed with known auxiliary masses attached to each of the junction points. The addition of these masses tends to increase the working of the local structure in the lower modes, or, equivalently, to lower the frequencies of the local structure

modes into the frequency range considered in the mode survey. The amount of mass loading which is required to accomplish this may be estimated by analysis of the particular substructure being tested. By the time hardware becomes available for vibration testing an analytical model will exist. The analyst can use the model to compute frequencies and modes using various values for mass loading and from these results select the minimum weights which will lower the frequencies of the local structure into the range of interest. Further verification of these weights by performing a synthesis using the mass loaded analytical component modes, and comparing the synthesis results with a direct analysis of the assembly is recommended.

It should be noted that the analytical model may not represent the local structure flexibilities very accurately. For this reason it is advisable to perform this above analysis using several values for local structure stiffnesses which cover the possible range, and to be conservative, select the largest mass loading required by these cases. A further check of these estimated values of mass loading may be obtained by applying a transient excitation to the added masses and observing the frequency content of the response. The mass loading may then be adjusted if required.

The synthesis of mass loaded modes is the same as for free-free modes, except that the kinetic energy due to the added junction point masses must not be included in the eigenvalue problem for the assembly. The physical mass matrix, when using mass loading, is

$$\left[M_x\right] = \left[M_x^S\right] + \left[M_x^L\right] \tag{21}$$

where $\left[M_x^S\right]$ is the mass matrix of the structure and $\left[M_x^L\right]$ is the mass matrix of the added weights. The second matrix will have zeros everywhere except for the diagonal elements corresponding to junction point motions. The

unccupled modal mass matrix is

$$\left[M_{\xi}^{S}\right] = \left[\varphi_{x}\right]^{T}\left[M_{x}^{S}\right]\left[\varphi_{X}\right] \tag{22}$$

instead of that given by Equation (3c). It should be noted that the component normal modes are not orthogonal with respect to $\left[M_{x}^{S}\right]$, and that the component modal mass matrices used to compute component modal stiffness by Equation (19) should include the mass due to the added weights. Equation (7b) is replaced by

$$\left[M_{\hat{\xi}}^{S}\right] = \left[T\right]^{T}\left[M_{\xi}^{S}\right]\left[T\right] \tag{23}$$

and the eigenvalue problem for the assembly is now

$$\left[K_{\hat{\xi}}\right]\left\{\varphi_{\hat{\xi}}\right\} = \omega_{\hat{\xi}}^{2}\left[M_{\hat{\xi}}^{S}\right]\left\{\varphi_{\hat{\xi}}\right\} \tag{24}$$

instead of that given in Equation (13). With the exception of these three equations, the synthesis of mass loaded modes is identical to that of free-free modes.

Fixed Junction Points

This is the most complicated of the coupling procedures, but the best from the standpoint of working the local structure in the component testing. The mode surveys are performed with the junction points held fixed, and therefore the substructure normal modes give displacements relative to the junction points. To obtain the absolute displacements, $\{x\}$ for a substructure,

we must add the displacements due to junction point motion, $\{\tilde{x}\}$, to the relative displacements, $\{\bar{\bar{x}}\}$:

$$\{x\} = \{\tilde{x}\} + \{\bar{\bar{x}}\} \tag{25a}$$

or partitioning,

$$\begin{Bmatrix} x^I \\ \hline x^J \end{Bmatrix} = \begin{Bmatrix} \tilde{x}^I \\ \hline x^J \end{Bmatrix} + \begin{Bmatrix} \bar{\bar{x}}^I \\ \hline 0 \end{Bmatrix} \tag{25b}$$

where the superscripts "I" and "J" designate internal and junction point displacements, respectively. A matrix $[\sigma]$ giving $\{\tilde{x}^I\}$ in terms of $\{x^J\}$ can be determined from additional testing, as will be shown shortly. Making use of $[\sigma]$, Equation (25b) becomes

$$\begin{Bmatrix} x^I \\ \hline x^J \end{Bmatrix} = \left[\begin{array}{c|c} \sigma & I \\ \hline I & 0 \end{array}\right] \begin{Bmatrix} x^J \\ \hline \bar{\bar{x}}^I \end{Bmatrix} \tag{25c}$$

This equation expresses the absolute displacements of the internal points and junction points as a function of the absolute junction point displacements and relative displacements of the internal points.

The relative displacements may be expressed in terms of the generalized coordinates associated with the substructure normal modes:

$$\{\bar{\bar{x}}^I\} = [\varphi_I^N]\{\xi^N\} \tag{26}$$

combining Equations (25c) and (26) gives

$$\begin{Bmatrix} x^I \\ x^J \end{Bmatrix} = \left[\begin{array}{c|c} \sigma & \varphi_I^N \\ \hline I & 0 \end{array}\right] \begin{Bmatrix} x^J \\ \xi^N \end{Bmatrix} \tag{27a}$$

or

$$\{x\} = [\varphi'_x] \{\xi'\} \tag{27b}$$

The component modal mass matrix is

$$[M'_\xi] = [\varphi'_x]^T [M_x] [\varphi'_x]$$

$$= \left[\begin{array}{c|c} M_\xi^{JJ} & M_\xi^{JN} \\ \hline M_\xi^{NJ} & M_\xi^{NN} \end{array}\right] \tag{28}$$

while the component modal stiffness matrix is

$$[K'_\xi] = \left[\begin{array}{c|c} K_\xi^{JJ} & 0 \\ \hline 0 & K_\xi^{NN} \end{array}\right] \tag{29}$$

where

$$\begin{bmatrix} K_\xi^{NN} \end{bmatrix} = \begin{bmatrix} M_\xi^{NN} \end{bmatrix} \begin{bmatrix} \omega^2 \end{bmatrix}$$

and $[\omega^2]$ is the diagonal matrix of circular frequencies squared. The $[K_\xi^{JJ}]$ matrix can be determined from static test, since it involves only junction point coordinates which are external to the substructure and can therefore be instrumented for force and displacement measurements.

The matrices $[K_\xi^{JN}]$ and $[K_\xi^{NJ}]$ are null. This follows from the definition of a generalized stiffness coefficient, K_{ij}, as the work done by generalized forces associated with the i^{TH} mode acting through displacements associated with the j^{TH} mode. The work done by junction forces on a normal mode displacement is zero since the junctions are fixed in a normal mode. Therefore $[K_\xi^{JN}]$ is null, and by symmetry $[K_\xi^{NJ}]$ is also null.

By definition, an element of $[\sigma]$, σ_{ij}, is the displacement at the i^{TH} internal coordinate due to a unit displacement of the j^{TH} junction point corrdinate, with all other junction point coordinates held fixed. This implies that a series of static tests could be used to determine $[\sigma]$ for redundant coupling, and that rigid body considerations can be applied for statically determinate coupling. In the static tests the junction point constraints would be removed, one at a time, and the unconstrained junction coordinate given a unit displacement. Measurement of the internal displacements would give $[\sigma]$, one column at a time. This is not, however, practical because of the difficulty involved in measuring displacements at many points. In addition to this, some of the internal points may not be accessible.

We can, however, take advantage of the fact that the structure is already instrumented with accelerometers, and determine $[\sigma]$ from additional mode survey data. The junction point constraints are removed, one at a time, and a shaker attached to the unconstrained junction point. The modal data obtained

from one such mode survey is used to calculate a static displacement shape, which when normalized so that the free junction coordinate has a unit displacement, is one column of $[\sigma]$. Details of this calculation are shown in the Appendix.

For a component with n junction point degrees of freedom the above formulation would require the determination of an n x n junction point stiffness matrix, $\left[K_{\xi}^{JJ}\right]$, from static test. An additional n mode survey would be required to obtain data to compute the columns of $[\sigma]$. A reduction in the amount of testing can be effected through the selection of a different set of generalized coordinates. The junction point displacements can be expressed as

$$\left\{X^{J}\right\} = \left[\varphi_{J}^{R}\right]\left\{\xi^{R}\right\} + \left[\varphi_{J}^{C}\right]\left\{\xi^{C}\right\} \tag{30}$$

where the subscript "J" refers to junction point coordinates and the superscripts "R" and "C" refer to rigid body and constraint modes, respectively. The total number of rigid body plus constraint modes is equal to the number of junction point degrees of freedom, n. If the number of rigid body modes is m; then $\left\{\xi^{C}\right\}$ is a vector containging n-m arbitrarily selected junction point displacements, and $\left[\varphi_{J}^{C}\right]$ is a matrix made up of ones and zeros. Each column of $\left[\varphi_{J}^{C}\right]$ contains one element which is unity while the rest are zeros. If the j^{TH} element of $\left\{\xi^{C}\right\}$ is the i^{TH} junction point displacement, then there will be a one at row i column j of $\left[\varphi_{J}^{C}\right]$.

Combining Equations (27a) and (30) yields

$$\begin{Bmatrix} x^I \\ \hline x^J \end{Bmatrix} = \left[\begin{array}{c|c|c} \sigma\, \varphi_J^R & \sigma\, \varphi_J^C & \varphi_I^N \\ \hline \varphi_J^R & \varphi_J^C & 0 \end{array}\right] \begin{Bmatrix} \xi^R \\ \hline \xi^C \\ \hline \xi^N \end{Bmatrix} \tag{31a}$$

or

$$\begin{Bmatrix} x^I \\ \hline x^J \end{Bmatrix} = \left[\begin{array}{c|c|c} \varphi_I^R & \varphi_I^C & \varphi_I^N \\ \hline \varphi_J^R & \varphi_J^C & 0 \end{array}\right] \begin{Bmatrix} \xi^R \\ \hline \xi^C \\ \hline \xi^N \end{Bmatrix} \tag{31b}$$

or

$$\{x\} = \left[\varphi_x^*\right]\{\xi^*\} \tag{31c}$$

The component modal mass matrix is

$$\left[M_\xi^*\right] = \left[\varphi_x^*\right]^T \left[M_x\right] \left[\varphi_x^*\right]$$

$$= \left[\begin{array}{c|c|c} M_\xi^{RR} & M_\xi^{RC} & M_\xi^{RN} \\ \hline M_\xi^{CR} & M_\xi^{CC} & M_\xi^{CN} \\ \hline M_\xi^{NR} & M_\xi^{NC} & M_\xi^{NN} \end{array}\right] \tag{32}$$

and the component modal stiffness matrix is

$$\left[K_\xi^*\right] = \begin{bmatrix} 0 & 0 & 0 \\ 0 & K_\xi^{CC} & 0 \\ 0 & 0 & K_\xi^{NN} \end{bmatrix} \tag{33}$$

where $\left[K_\xi^{NN}\right]$ is the same as in Equation (29) and $\left[K_\xi^{CC}\right]$ is determined from static test, as was $\left[K^{JJ}\right]$ of Equation (29). It should be noted that $\left[K_\xi^{CC}\right]$ is an (n-m) x (n-m) matrix while $\left[K_\xi^{JJ}\right]$ is an n x n matrix. The matrices $\left[K_\xi^{CN}\right]$, and $\left[K_\xi^{NC}\right]$ are null for the same reason the $\left[K_\xi^{JN}\right]$ and $\left[K_\xi^{NJ}\right]$ of Equation (29) were null. The submatrices in the first row and column are null since there is no strain energy in a rigid body mode.

The rigid body modes, $\left[\varphi_I^R\right]$ and $\left[\varphi_J^R\right]$, can be easily written by the analyst, while the submatrix $\left[\varphi_I^C\right]$ is the product of $\left[\sigma\right]$ and $\left[\varphi_J^C\right]$. It is not, however necessary to determine the entire $\left[\sigma\right]$ matrix, since the postmultiplication of $\left[\sigma\right]$ by $\left[\varphi_J^C\right]$ amounts to picking out n-m columns of $\left[\sigma\right]$. Only n-m additional mode surveys are required to determine the n-m columns of $\left[\varphi_I^C\right]$. If the connection between substructures is statically determinate, then no constraint modes are required, and no static testing or additional mode surveys are needed. Because of the reduction in the amount of testing required, it is advantageous to use the component mode transformation of Equation (31b), and the modal mass and stiffness matrices of Equations (32) and (33) in the synthesis. Once these matrices have been obtained, the synthesis calculations can be performed as shown in the section entitled "General Coupling Procedures".

It can be seen that the use of fixed junction point modes requires considerable additional testing and analysis to determine the constraint modes if the components are redundantly connected. In addition to this, there is also the problem of determining the damping values associated with the constraint modes. This subject is discussed in Reference 1.

Fixed Base

This procedure rivals the previous one in complexity, although it does not offer the advantage of working the local structure near the junction points. In fact, the results obtained from using fixed base component modes to compute free-free assembly modes are no better, and usually poorer, than those obtained with free base component modes. The use of fixed base modes is not therefore recommended unless test considerations dictate.

When using fixed base modes, a component mode survey is performed with the base held fixed and the junction points free or mass loaded. (The base is defined here to mean any part of the substructure other than the junction points.). Therefore the substructure normal modes give displacements relative to the base. As with fixed junction point modes, the absolute displacements in a substructure are expressed as the sum of the relative displacements and the displacements due to the motion of the base. The analytical development for fixed base modes is identical to that for fixed junction point modes as shown in the previous section. With the substitution of the sub and superscript "B", designating base, for "J", which denotes junction point, the equations of the previous section hold for fixed base components. If the fixity is redundant, constraint modes must be used along with rigid body and elastic modes to represent the displacements.

ANALYTICAL VERIFICATION

The coupling procedures formulated in the previous section were first applied to two analytical check problems so that verification and comparison of the various techniques could be performed without introducing the uncertainties associated with test data. The substructure modal properties were computed, as were those of the assembly, from lumped parameter idealizations of the components and assembly. The modal properties of the substructures were used as input data for the coupling analysis, while the direct analysis of the assembly was performed in order to provide results with which to compare those obtained from synthesis.

Grumman's COMAP/ASTRAL system, which combines a structural analysis program (ASTRAL) with a matrix language (COMAP), was employed to perform these analyses. This system is well suited to this purpose, since the coupling procedures are merely a series of matrix operations which are easily coded in the COMAP language. In addition to this, the stiffness matrices can be generated, and the eigenvalue problems solved for the assembly as well as the components, all within the same program.

Orbiter/Tank Coupling

The first analytical check problem represents orbiter-to-tank coupling for a "series-burn" configuration which was under serious consideration by Grumman at the time that this problem was selected. Figure 1 shows the idealization, which considers pitch-plane motion only, with the orbiter having seven mass points, and the tank being represented with eleven mass points. The problem features redundant connections between the two components as well as local structure flexibility.

There are two degrees of freedom at each point (longitudinal and lateral displacement) and thus the orbiter and tank idealizations contain fourteen and twenty-two degrees of freedom, respectively. Since the orbiter and tank are coupled by pins at the three junction points, the coupled system has thirty degrees of freedom. It should be noted that the junction points are offset from the fuselage center lines, and connected to the fuselage masses through flexible members which represent the local structure flexibility.

The coupling procedures were applied to this problem for seven different combinations of substructure boundary conditions. These boundary conditions are:

1. A free-free tank coupled to a free-free orbiter.
2. A free-free tank coupled to a free-free orbiter, with the junction points of both components mass loaded.
3. A free-free tank coupled to an orbiter supported from its junction points.
4. A free-free tank coupled to an orbiter supported from its junction points, with the tank junction points mass loaded.
5. A free-free orbiter coupled to a tank supported at its base with the junction points of both components mass loaded.
6. An orbiter supported at its junction points coupled to a tank supported at its base, with the tank junction points mass loaded.
7. A tank supported from its junction points coupled to an orbiter supported from its junction points.

The free-free assembly modes were synthesized from component modes having all seven combinations of boundary conditions listed above. In order to check the coupling procedures, all of the substructure modes were employed in the initial coupling analyses. As expected, the results obtained using all substructure modes were identical, except for roundoff, to those obtained by direct solution of the eigenvalue problem for the assembly.

Since in a practical case, only a limited number of substructure modes will be available, the synthesis procedures were next applied using a reduced number of component modes. Results obtained using sixteen and ten total substructure modes are shown in Tables 1, 2, 4 and 5. An equal number of modes was used to represent each substurcture, e.g., eight orbiter modes and eight tank modes were used for the cases having sixteen total modes. The three rigid body modes per substructure are not included in the total number of component modes. This figure represents only normal and constraint modes. Thus for a free-free substructure represented by eight modes, these modes are the lowest eight normal modes, while for a component supported at its base or junction points, the eight modes would be made up of the lowest five normal modes and three constraint modes. This method of counting the component modes provides a fair basis for comparison, since the three rigid body modes of the assembly are not included in the results presented.

A synthesis performed using sixteen substructure normal and constraint modes along with six rigid body modes will yield thirteen elastic modes and three rigid body modes for the assembly. This is due to the fact that six of the component modes are used to establish junction point compatibility. Similarly, seven assembly elastic modes can be computed using ten component normal and constraint modes.

Table 1 shows a comparison between the assembly frequencies obtained from synthesis using substructure modes with boundary conditions one through four, and those obtained from direct analysis of the assembly. The results obtained using fee-free modes for both components (boundary condition #1) are very poor. Only the first frequency is close to that of the direct solution when sixteen substructure modes are used, and there are no good frequencies obtained with ten substructure modes. This is due to the fact that the local structure is not worked in the lower component modes.

The addition of mass loading to the junction points of both free-free substructures improves the situation significantly. Results obtained using these component modes (boundary condition #2) show that the first seven assembly frequencies can be computed reasonably well using sixteen component modes, and the first two frequencies can be computed from ten substructure modes.

Results obtained using free-free tank modes along with fixed junction point orbiter modes (boundary condition #3) are as poor as those computed using free-free modes (boundary condition #1). Here again this is due to not working the local structure of the tank, even though that of the orbiter is worked by the supports. The use of mass loading at the tank junction points (boundary condition #4) yields results which are much better, and comparable to those of boundary condition #2.

Frequencies calculated for fixed base tank modes are shown in Table 2. These include a free-free orbiter with mass loaded junction points coupled to a tank with mass loaded junction points supported at its base (boundary condition #5), and an orbiter supported at its junction points coupled to a fixed base tank with mass loaded junction points (boundary condition #6). It should be noted that the last three frequencies shown in Table 2 differ from those of Table 1. This is due to a slight difference in the mathematical model of the tank used to obtain the results in these tables. The tables are, however, consistent within themselves. Comparison of the frequencies obtained from synthesis with those of the direct solution shows the results for these boundary conditions to be uniformly poor. Only one frequency is computed correctly using sixteen substructure modes, while none are calculated with ten component modes. These poor results are not caused by failure to work the local structure in the component modes, since all junction points are either fixed or mass loaded.

The data shown in Table 3 will help explain the difficulty. This table contains the free-free frequencies of the tank as computed from direct analysis of the tank, and by representing the tank in terms of its fixed base normal modes, constraint modes, and rigid body modes. The second calculation involves the solution of the eigenvalue problem associated with the component mass and stiffness matrices in the component modal coordinate system. This is the same representation of the tank employed in the synthesis, and therefore the intermediate calculation indicates how well the free-free tank is approximated in the synthesis. Examination of the results shows that only the first three free-free tank modes are accurately represented when eight fixed base modes (five normal modes and three constraint modes) are used, and that none of the free-free modes are represented when five fixed base modes (two normal modes) are employed. This explains the poor results shown in Table 2.

Table 4 contains results obtained by coupling a tank supported from its junction points to an orbiter supported at its junction points (boundary condition #7). These results are essentially the same as those obtained for boundary conditions #2 and #4. It should not, however, be concluded from this that mass loading is always as effective in working the local structure as fixing the junction points. This is true if sufficiently large masses are used, but there are practical limitations on the amount of mass which may be attached to the junction points in a test.

The data presented in Table 5 is intended to demonstrate that the results obtained from modal synthesis are highly dependent on the nature of the substructures being coupled. The orbiter/tank problem was modified by stiffening the members which represent the local structure in both the orbiter and the tank. Comparison of the data contained in Table 5 with that of Table 1 shows that, as expected, the assembly frequencies have been raised by stiffening the local structure. The important thing to note, however, is the

great improvement in the synthesis results obtained using free-free modes for both components (boundary condition #1), due to the fact that the stiffer local structure is not significantly deformed in the lower assembly modes, and therefore the lack of local structure deformation in the component modes is not important. This demonstrates one way in which the nature of the structure, in this case the local structure stiffness, effects the coupling analysis. Another situation will be encountered in the next check problem.

Results presented here demonstrate that the coupling procedures developed can be successfully applied to a representative problem using calculated modal data. It was also shown that the results obtained using free-free modes can be significantly improved through the use of mass loaded or fixed junction points, and that the results obtained using fixed base modes are poor.

Orbiter/Booster Coupling

The second analytical check problem is the Langley 1/15 scale dynamic model of a Space Shuttle configuration which is made up of an orbiter and a booster. This problem is the same as that described in Reference 6, except for the addition of a third spring assembly, half way between the two existing ones, and the use of pins to connect the orbiter with the spring assemblies when coupling the components. The third spring assembly was added in order to provide redundant coupling in the pitch direction, while the reason for using pins is related to the fact that this structure was also employed in the experimental verification discussed in the next section. If the original connections which had moment continuity had been retained, the synthesis procedures would require that the mode shapes contain junction point slopes

as well as junction point displacements. Because of the difficulties involved in slope measurement, the connections were modified. Calculation and coupling of analytical modes for the 1/15 scale model will be discussed here, while the synthesis of the test modes for this structure is treated in the following section.

Figure 2 shows the orbiter, booster and coupled orbiter/booster. Both fuselages are tubes with concentrated lead weights to simulate propellant. The orbiter is 1.93 meters (76 inches) long and has a mass of 40.8 kilograms (90 lbs.), while the booster is 3.43 meters (135 inches) long, with a total mass of 130.2 kilograms (287 lbs.). The three spring assemblies which are attached to the booster may be considered to represent local structure flexibility, and are included as part of this substructure when calculating booster modes. A more detailed description of the structures is contained in Reference 6.

The lumped parameter idealization considers pitch-plane motion only, and employs ten degrees of freedom to represent the orbiter, twenty for the booster, and twenty-four for the coupled orbiter/booster. These degrees of freedom are represented by arrows in Figure 2. It should be noted that six degrees of freedom are used to represent junction point motions on both the orbiter and booster. This was done because the component mode shapes must contain all junction point displacements in order to establish junction point compatibility in the synthesis analysis. The booster junction points are located at the ends of the spring assemblies, while the orbiter junction points are offset from the fuselage centerline through rigid links. The sparcity of longitudinal degrees of freedom on the fuselages is due to the fact that the flexible longitudinal fuselage modes have frequencies which are above the range of interest for this study.

The fuselage mass and elastic properties used on the analysis were obtained from Reference 6, as were the spring assembly stiffness matrices, which were taken from the 10^4 nominal case. The masses of the spring assemblies were lumped at the fuselage center line and at the tips of the spring assemblies. The proportion to be lumped at the tips of the spring assemblies were determined by matching the analytical results to test results for booster modes showing large motions of the spring assemblies. This is very important to the coupling, since the spring assembly modes are, in this problem, the local structure modes.

Table 6 shows the frequencies of the component elastic modes used in the synthesis, along with descriptions of the associated mode shapes. Although frequencies obtained from both analysis and test are presented in this table, the discussion of the test data, where it differs from the analytical data, is reserved for the next section.

Only the first and second orbiter bending modes were used in the synthesis, since the third orbiter mode was above the frequency range of interest. Table 6A shows those frequencies as obtained from analysis and test of the free-free orbiter, while the mode shapes are plotted in Figures 3 and 4. Although modes were plotted from test data, the analytical mode shapes show the same character.

Nine free-free booster modes were employed in the synthesis. Table 6B lists the frequencies of these modes and Figures 5 through 13 show the mode shapes as determined by test. The first two modes are the first and second fuselage bending modes. The next three modes are "spring axial" modes. These are modes in which the booster fuselage stands still and the orbiter ends of the spring assemblies move parallel to the axis of the fuselage (see Figures 7, 8 and 9). Mode number 6 is the third fuselage bending, and modes 7, 8 and 9 are "spring lateral" modes. These are similar to the "spring axial"

modes except that the spring motion is perpendicular to the axis of the fuselage (see Figures 11, 12 and 13). The "spring axial" and "spring lateral" modes are very important to the synthesis, since they represent local structure motion. This will be demonstrated shortly.

Table 6C presents the frequencies of the mass loaded booster and Figures 14 through 21 show the experimental mode shapes. It is interesting to compare these frequencies with those of the free-free booster, to see the effect of mass loading. Mass loading has lowered the frequencies of the "spring axial" and "spring lateral" modes. The mass loaded "spring axial" frequencies are all below 67 Hz, as opposed to the free-free "spring axial" frequencies which were above 145 Hz. The mass loaded "spring lateral" frequencies are below 80 Hz as compared with the free-free "spring lateral" frequencies which were above 209 Hz. If modes above 100 Hz were left out of the synthesis, the free-free results would not include any spring or local structure modes, while the mass loaded results would include all six of these modes. Mass loaded synthesis using these modes would then produce good results, while the free-free synthesis would yield nonsense.

It should be noted that the structure considered here is not typical and does not fully demonstrate the advantage of mass loading. Because there are so few fuselage frequencies below the local structure frequencies, a significant reduction in the local structure frequencies through mass loading does not markedly reduce the total number of booster modes which must be taken in order to include the local structure modes. All local structure modes are included in the first 9 free-free modes while the first 7 mass loaded modes include all of the local structure modes. In a more typical structure, a similar reduction in local structure frequencies would produce a greater reduction in the mode numbers of the local structure modes, and therefore a far more significant reduction in the total number of component modes required for synthesis.

Coupled orbiter/booster modes were synthesized using the component elastic modes along with rigid body modes. Free-free orbiter modes were coupled with free-free booster modes and mass loaded booster modes. The mass loaded booster had a mass of approximately 5.9 kilograms (13 lbs.) attached to the orbiter end of each spring assembly. There was no point in mass loading the orbiter, since all of the local structure flexibility is in the spring assemblies which are attached to the booster. Fixed base modes were not used due to the poor results they yielded for the orbiter/tank synthesis, while fixed junction point modes were omitted because of their complexity and doubtful advantage over mass loaded modes.

Table 7 presents a comparison of coupled orbiter/booster frequencies as computed by: direct analysis, synthesis of free-free analytical modes, and synthesis using mass loaded analytical modes. Mode shapes obtained from the direct analysis are shown in Figures 22 through 27. For both mass loaded and free-free synthesis, frequencies obtained using 11 substructure modes (2 orbiter modes and 9 booster modes) compare well with those computed directly. This was expected, since, as previously shown, the first 9 booster modes include all 6 local structure modes. The synthesis results obtained using only 8 substructure modes (2 orbiter modes and 6 booster modes) are another story. The free-free synthesis results are quite poor, and, while the mass loaded synthesis results are significantly better, they are not as good as those obtained using 11 substructure modes. The reason for this is again obvious from the previous discussion of the component modes. The first 6 free-free booster modes do not include any of the 3 spring lateral modes, while the first 6 mass loaded booster modes include 2 of the 3 spring lateral modes. Once again, this demonstrates the importance of local structure modes in the synthesis and the advantage of using mass loading to reduce the number of component modes required for synthesis.

Unlike the first analytical check problem, this one lends itself well to free-free coupling, and therefore the improvement obtained through the use of mass loading is not as significant. This is because the actual (or original) junction point masses were large enough to work the local structure to a significant extent, which was not the case in the orbiter/tank synthesis.

EXPERIMANTAL VERIFICATION

As a final demonstration and verification of the synthesis techniques formulated in this report, modal data obtained from substructure tests were synthesized. The Langley 1/15 scale model described in the previous section and shown in Figure 2 was used in this effort. Orbiter, booster, and coupled orbiter/booster modal properties were determined from mode surveys of the individual components and the assembly. The modal properties of the substructures were used as input data for the coupling analysis, while the assembly mode survey was performed in order to provide results with which to compare those obtained from synthesis. The coupling analyses were performed using Grumman's COMAP/ASTRAL system which was described briefly in the section on orbiter/tank analytical coupling.

The structures were instrumented for pitch plane motion only, and employed ten transducers for the orbiter, twenty for the booster, and twenty-four for the coupled orbiter/booster. The transducers are represented by arrows in Figure 2, and are the same as the degrees of freedom employed in the analysis.

Table 6 presents the frequencies of the component elastic modes, as obtained from both test and analysis, along with descriptions of the associated mode shapes. The component mode shapes obtained from mode survey data are plotted in Figures 3 through 21. The reader is referred back to the discussion of this table in the previous section, since only differences between analytical and test data will be pointed out here. There is generally good agreement between the two sets of data, except that the third mass loaded booster mode, a spring axial mode, is not present in the test data. The consequences of this will be seen from the synthesis results obtained using these modes.

The component elastic and rigid body modes were coupled to obtain the modal data for the assembly. Substructure boundary conditions were the same as those of the second analytical check problem.

Table 8 presents a comparison of coupled orbiter/booster frequencies as determined from :direct test of the coupled structure, synthesis using modal data from free-free tests, and synthesis using mass loaded modal test data. Assembly mode shapes obtained from direct test are plotted in Figures 28 through 32. The first and second modes are missing from the direct test data, but are included in the plots of analytical mode shapes in Figures 22 through 27. Synthesized mode shapes obtained using free-free test modes are contained in Figures 33 through 39, while those obtained with mass loaded test modes are presented in Figures 40 through 46. The third mode shape was computed using analytical spring axial modes, for reasons to be discussed shortly. The first 7 synthesized frequencies obtained using 11 free-free test modes (2 orbiter modes and 9 booster modes) compare well with those obtained from direct test. Those obtained using 12 mass loaded modes (2 orbiter modes and 10 booster modes) are not as good. The second frequency does not compare as well as that computed using free-free modal data, and the third mode is missing completely.

Examination of the mode shapes for these two modes shows that they both possess the same characteristic: The orbiter and booster move in opposite directions axially (see Figs. 23&24). This type of motion is small in the second mode, but a dominant characteristic of the third mode. Due to the fact that one of the "spring axial" modes was missing from the mass loaded test data, it is impossible to synthesize modes having this characteristic. The fact that this is a problem is demonstrated by the frequencies shown in the last column.

These results were obtained by using 3 "spring axial" modes from analysis along with the mass loaded test modes. It can be seen that the second frequency improves and the third one, which was missing, is now present.

The results presented here demonstrate that the modes of an assembly can be synthesized from mode survey data for the individual components. Because of the missing third mode of the mass loaded booster, the effect of mass loading could not be evaluated. It is, however, safe to assume that it would be the same as for the analytical coupling.

CONCLUSIONS AND RECOMMENDATIONS

It has been demonstrated in this study that the frequencies and mode shapes of an assembly can be synthesized from mode survey data for the individual components. Modal coupling has been successfully accomplished using both free-free and mass loaded test modes. No elastic analysis was required to supplement the test data, even though the 1/15 scale space shuttle model used had redundant connections. The component mode surveys were of the same type as the usual mode surveys to obtain free-free modes, and the use of mass loading added only slight complication.

Synthesis using free-free component modes proved to be the simplest from the standpoint of component testing as well as analytical coupling. The convergence of the synthesis procedure was, however, poorer than that obtained using mass loaded or fixed junction point component modes. This was due to the fact that mass loading provides a more realistic "working" of the local structure adjacent to the junction points in the lower component modes, and therefore these mode shapes include more of the local structure deformations. If sufficient mass is employed, convergence is comparable to that obtained using fixed junction point component modes. Practical considerations do, however, limit the amount of mass, and therefore the convergence is usually not as good as that obtained for fixed junction points. Mass loaded synthesis is only slightly more complicated than free-free synthesis, however, and a great deal less complicated than fixed junction point synthesis. In the latter procedure, considerable additional testing and analysis are required to determine the constraint modes. In addition to this, the determination of damping values associated with the constraint modes presents a problem.

Synthesis using fixed base component modes has all of the disadvantages associated with fixed junction point modes, but does not have the advantage of working the local structure. Convergence is no better, and usually poorer than that obtained with free base component modes. The use of fixed

both component modes in not recommended. They should only be used when test considerations dictate.

Fixed junction point component modes are recommended only when the substructure connections are statically determinate. When the components are redundantly connected the improved convergence obtained by fixing the junction points is more than offset by the added complication, and the use of mass loaded modes is recommended, even though a greater number of them may be required. Free-free component modes may also produce acceptable results for some structures.

It should be noted that while the above statements about the relative merits of the various coupling procedures are true in general, the extent to which they are important is highly dependent on the nature of the structure. If the local structure is very stiff, and does not deform significantly in the lower modes of the assembly, then there is no need for the component modes to reflect local structure motion, and there is in turn no advantage to using mass loaded or fixed junction point modes over free-free modes. If the junction points are sufficiently heavy, and/or the local structure is sufficiently flexible, then the local structure will be naturally "worked" in the lower free-free modes, and again there is no need for fixing or mass loading the junction points.

Care must be taken when performing the component mode surveys to insure that all of the substructure modes of interest are obtained, and that the data is accurate. If a component mode is inaccurately measured, or missing altogether, then one or more of the assembly modes may be missing or poorly represented when the data is synthesized. This is particularly true when the missing or inaccurate mode is a local structure mode. It should , however, be pointed out that modes can be missed or inaccurately measured in an assembly mode survey.

Since the results produced by modal coupling procedures are so highly dependent on the nature of the substructures being coupled, it is recommended that if there is continued interest in using modal coupling for the Space Shuttle program, a modal coupling study be performed using test data from the Langley second generation Shuttle dynamic model. The second generation model is much more representative of the final shuttle configuration than the 1/15 scale model used in this study, and therefore conclusions drawn from the new model would be more relevant to the actual shuttle.

where

$$\left[k\right] = \left[\varphi\right]^T \left[K\right]\left[\varphi\right] = \text{the modal stiffness matrix} \qquad \text{(A-3b)}$$

$$\left\{f\right\} = \left[\varphi\right]^T \left\{F\right\} \qquad \text{(A-3c)}$$

The mode shapes and modal stiffnesses are obtained from a vibration survey performed with all but one junction point coordinates held fixed. There are no external forces other than the shaker force, F_J, applied at the free junction point. Partitioning Equation (A-3c) gives

$$\left\{f\right\} = \left[\varphi_I^T \;\vdots\; \varphi_J^T\right] \left\{\begin{matrix} F_I \\ \hline F_J \end{matrix}\right\} \qquad \text{(A-4)}$$

where the subscripts "I" and "J" refer to internal degrees of freedom and the junction degree of freedom, respectively. It should be noted that φ_J^T is a column vector. Since $\left\{F_I\right\}$ is zero,

$$\left\{f\right\} = \left\{\varphi_J^T\right\} F_J \qquad \text{(A-5)}$$

Substituting Equation (A-5) into Equation (A-3a), and solving for $\left\{\xi\right\}$ yields

$$\left\{\xi\right\} = \left[k\right]^{-1} \left\{\varphi_J^T\right\} F_J \qquad \text{(A-6)}$$

and making use of Equation (A-2) gives

$$\left\{ x \right\} = \left[\varphi\right]\left[k\right]^{-1} \left\{ \varphi_J^T \right\} F_J \qquad \text{(A-7)}$$

This is the static deflection shape due to a load, F_J, applied at the free junction point. It should be noted that $\left[k\right]$ is not obtained from Equation (A-3b), but by taking the product of modal mass and circular frequency squared. This shape will now be normalized so that x_J , the junction point displacement, is unity. From Equation (A-7)

$$x_J = \beta \; F_J \qquad \text{(A-8a)}$$

where

$$\beta = \left\{ \varphi_J^T \right\}^T \left[k\right]^{-1} \left\{ \varphi_J^T \right\} \qquad \text{(A-8b)}$$

and $\left\{ \varphi_J^T \right\}^T$ is a row vector. Solving Equation (A-8a) for F_J, substituting in Equation (A-7), and setting $x_J = 1$ give a column matrix for the internal deflection shape due to a unit junction point displacement. Repeating this operation with each junction point free gives the entire desired matrix $\left[\sigma\right]$.

REFERENCES

1. Hasselman, T. K.: Study of Modal Coupling Procedures for the Space Shuttle: A Matrix Method For Damping Synthesis, NASA CR-112253, 1972.

2. Hurty, W. C.: Dynamic Analysis of Structural Systems Using Component Modes, AIAA Journal, Vol. 3, No. 4, April 1965.

3. Hou, S.: Review of Modal Synthesis Techniques and a New Approach, Shock and Vibration Bulletin, No. 40, Part 4, December 1969.

4. Benfield, W. A. ; and Hruda, R. F.: Vibration Analysis of Structures by Component Mode Substitution, AIAA Journal, Vol. 9, No. 7, July 1971.

5. Craig, R. R. Jr.; and Bampton, M. C. C.: Coupling of Substructures for Dynamic Analyses, AIAA Journal, Vol.6, No. 7, July 1968.

6. Thornton, E. A.: Vibration Analysis of a 1/15 Scale Dynamic Model of a Space Shuttle Configuration, NASA CR-111984.

TABLE 1

COUPLED ORBITER/TANK

ELASTIC FREQUENCIES - RAD/SEC

		SYNTHESIS							
		(1) Free - Free Tank to Free - Free Orbiter		(2) Free - Free Tank with Mass Loading to Free - Free Orbiter with Mass Loading		(3) Free - Free Tank to Fixed Junction Point Orbiter		(4) Free - Free Tank with Mass Loading to Fixed Junction Point Orbiter	
Mode No.	Direct Solution	16 Modes	10 Modes	16 Modes	10 Modes	16 Modes	10 Modes	16 Modes	10 Modes
1	14.02	14.85	23.02	14.02	14.19	14.72	17.8	14.02	14.18
2	15.77	22.40	27.20	15.77	15.92	17.99	19.19	15.77	15.87
3	33.83	62.77	65.38	33.83	49.38	47.48	65.43	33.83	51.11
4	38.01	65.95	73.70	38.02	136.2	52.48	72.66	38.01	142.3
5	65.80	81.32	121.9	65.81	180.7	65.83	164.2	65.81	163.7
6	72.72	152.8	169.6	75.96	326.9	80.18	258.8	74.76	320.7
7	80.72	168.7	191.9	81.19	402.0	89.02	304.0	81.20	402.5
8	81.86	194.0		168.1		224.0		190.8	
9	152.8	285.1		398.4		259.2		400.5	
10	194.1	291.1		400.4		289.6		402.4	
11	247.3	419.4		490.9		291.0		517.8	
12	289.1	422.7		636.9		401.7		676.6	
13	291.1	428.3		761.7		404.8		698.5	

TABLE 2

COUPLED ORBITER/TANK
ELASTIC FREQUENCIES - RAD/SEC

		SYNTHESIS			
		(5) Free-Free Oribiter with Mass Loading to Fixed Base Tank with Mass Loading		(6) Fixed Junction Point Orbiter to Fixed Base Tank with Mass Loading	
Mode No.	Direct Solution	16 Modes	10 Modes	16 Modes	10 Modes
1	14.02	14.83	18.97	14.83	18.48
2	15.77	18.36	29.17	18.23	29.37
3	33.83	51.58	83.28	51.60	83.14
4	38.01	53.92	126.3	53.89	128.4
5	65.80	75.53	491.1	75.54	491.5
6	72.72	81.06	597.1	80.61	593.5
7	80.72	143.5	662.6	143.8	662.2
8	81.87	252.5		236.8	
9	152.8	399.4		401.4	
10	194.1	405.4		404.2	
11	248.5	492.0		489.6	
12	418.4	599.2		599.2	
13	423.4	664.5		667.2	

TABLE 3

FREE-FREE TANK ELASTIC FREQUENCIES (RAD/SEC)

		Computed From Fixed Base Modes	
Mode No.	Direct Solution	8 Modes	5 Modes
1	29.13	29.14	68.59
2	29.54	29.54	124.3
3	30.18	30.27	597.5
4	55.47	75.95	663.4
5	61.78	133.8	19308.
6	66.12	598.3	
7	69.24	665.2	
8	88.79	19393.	

TABLE 4

COUPLED ORBITER/TANK

ELASTIC FREQUENCIES - RAD/SEC

		SYNTHESIS (7) Fixed Junction Point Tank to Fixed Junction Point Orbitor	
Mode No.	Direct Solution	16 Modes	10 Modes
1	14.02	14.01	14.07
2	15.77	15.77	15.84
3	33.83	33.83	52.13
4	38.01	38.02	148.4
5	65.80	65.81	196.9
6	72.72	74.76	296.9
7	80.72	81.20	402.1
8	81.86	190.8	
9	152.8	400.4	
10	194.1	402.1	
11	247.3	522.0	
12	289.1	680.7	
13	291.1	697.8	

TABLE 5

COUPLED ORBITER/TANK
ELASTIC FREQUENCIES - RAD/SEC
(STIFFENED LOCAL STRUCTURE)

		SYNTHESIS (1) Free-Free Tank to Free-Free Orbiter	
Mode No.	Direct Solution	16 Modes	10 Modes
1	23.40	23.46	24.64
2	58.73	59.14	61.45
3	67.09	67.32	69.99
4	87.88	88.83	106.1
5	170.0	172.1	178.0
6	172.1	176.3	223.0
7	211.6	216.9	338.6
8	218.7	221.9	
9	376.6	384.3	
10	573.7	591.6	
11	794.3	816.0	
12	937.2	952.9	
13	1164.	1167.	

TABLE 6

ORBITER/BOOSTER COMPONENT ELASTIC MODES

6A - Free-Free Orbiter Modes			
Mode No.	Frequency - HZ (Analysis)	Frequency - HZ (Test)	Mode Description
1	100.	102.	First Bending
2	204.	221.	Second Bending

6B - Free-Free Booster Modes			
Mode No.	Frequency - HZ (Analysis)	Frequency - HZ (Test)	Mode Description
1	35.0	38.0	First Bending
2	106.	102.	Second Bending
3	145.	146.	Spring Axial
4	152.	152.	Spring Axial
5	161.	163.	Spring Axial
6	191.	184.	Third Bending
7	209.	211.	Spring Lateral
8	216.	221.	Spring Lateral
9	225.	225.	Spring Lateral

6C - Mass Loaded Booster Modes			
Mode No.	Frequency - HZ (Analysis)	Frequency - HZ (Test)	Mode Description
1	31.7	34.0	First Bending
2	57.5	52.8	Spring Axial
3	60.4	----	Spring Axial
4	66.2	65.4	Spring Axial
5	79.5	71.3	Spring Lateral
6	84.1	76.4	Spring Lateral
7	92.7	81.5	Spring Lateral
8	115.	110.	Second Bending
9	203.	203.	Third Bending
10	244.	257.	Axial

TABLE 7

COUPLED ORBITER/BOOSTER

ELASTIC FREQUENCIES - HZ

(ANALYTICAL MODES)

		FREE-FREE SYNTHESIS		MASS LOADED SYNTHESIS	
Mode No.	Direct Analysis	8 Modes 2 Orbiter 6 Booster	11 Modes 2 Orbiter 9 Booster	8 Modes 2 Orbiter 6 Booster	11 Modes 2 Orbiter 9 Booster
1	25.9	29.3	26.0	26.2	26.1
2	37.3	49.0	37.3	37.6	37.5
3	52.7	86.7	52.7	53.7	53.0
4	99.2	120.	102.	110.	99.4
5	113.	170.	113.	200.	113.
6	120.		122.		120.
7	201.		202.		201.

TABLE 8

COUPLED ORBITER/BOOSTER

ELASTIC FREQUENCIES - HZ

(TEST MODES)

		FREE-FREE SYNTHESIS	MASS LOADED SYNTHESIS	
Mode No.	Direct Test	11 Modes 2 Orbiter 9 Booster	12 Modes 2 Orbiter 10 Booster	12 Modes* 2 Orbiter 10 Booster
1	26.0	26.4	26.4	26.6
2	38.7	38.4	42.0	39.3
3	57.6	55.0	----	49.9
4	92.3	98.3	90.5	89.4
5	108.	110.	106.	104.
6	125.	129.	111.	111.
7	185.	190.	203.	203.

* Using Analytical "Spring Axial" Modes

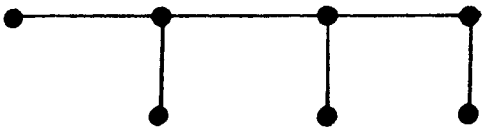

ORBITER

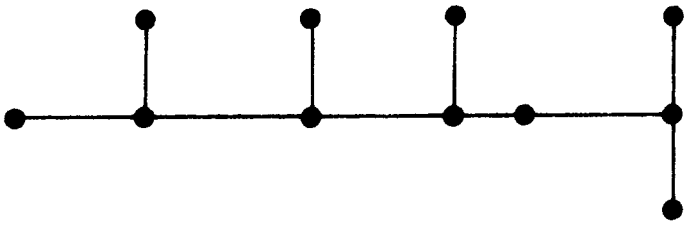

TANK

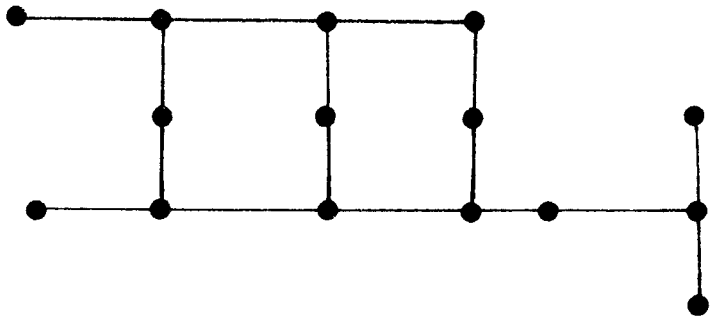

COUPLED ORBITER/TANK

IDEALIZATION OF ORBITER, TANK, AND COUPLED ORBITER/TANK

FIGURE 1

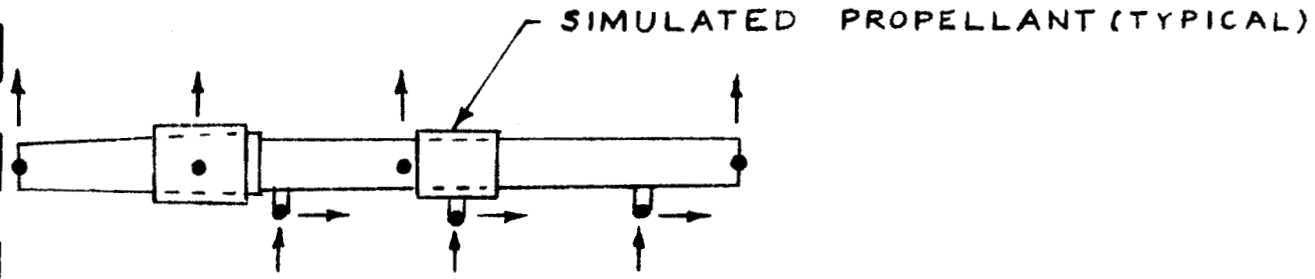

ORBITER

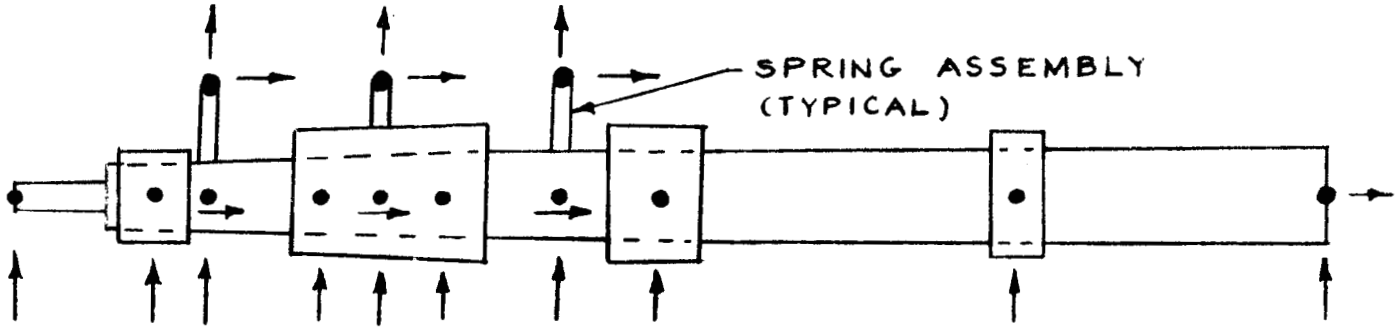

BOOSTER

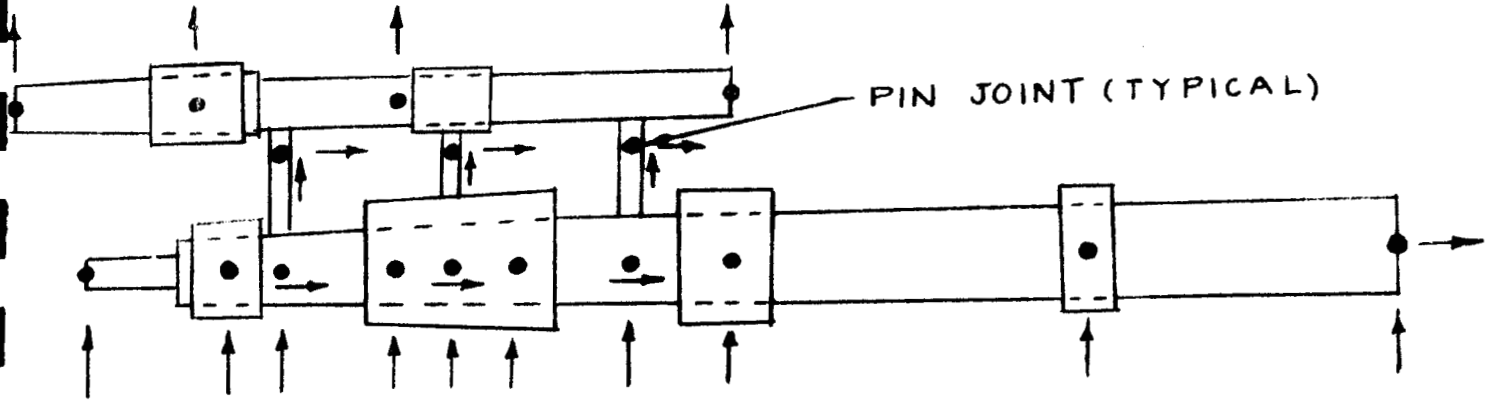

COUPLED ORBITER/BOOSTER

1/15 SCALE MODEL OF A SPACE SHUTTLE CONFIGURATION

FIGURE 2

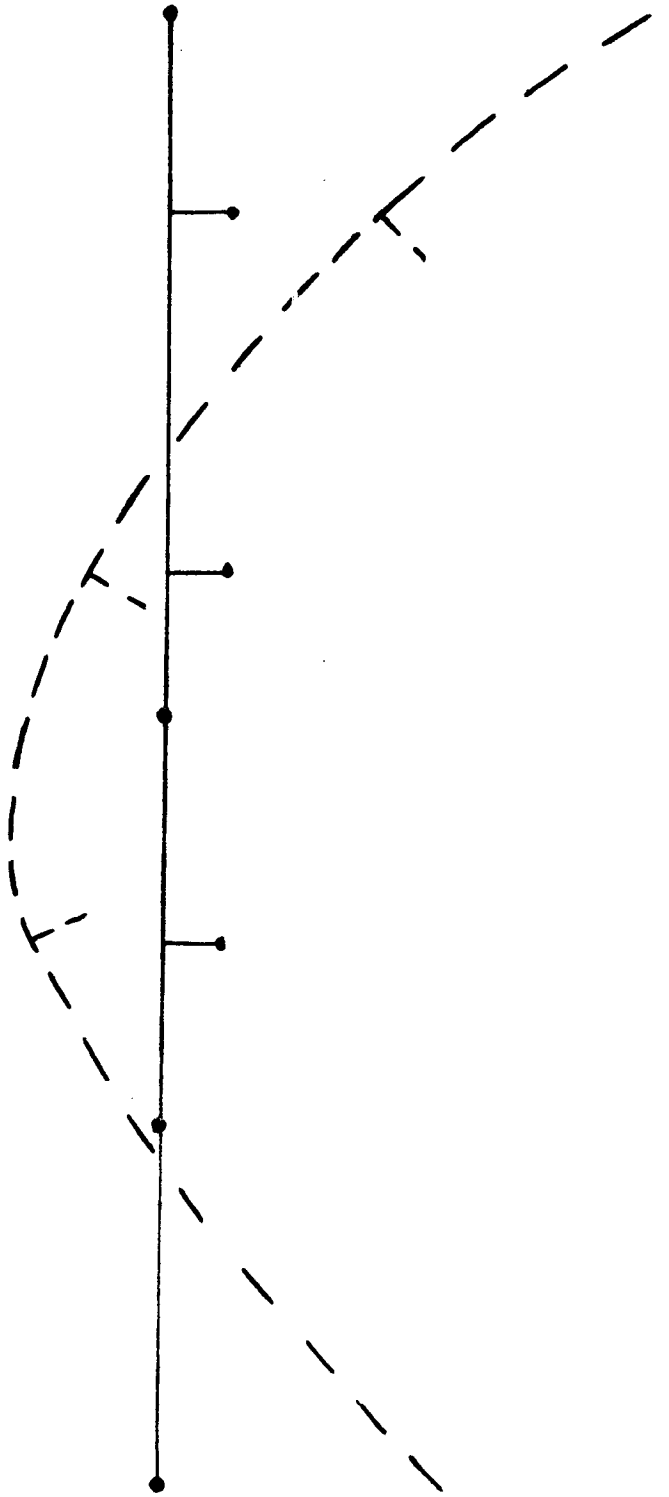

FIGURE 3 - FIRST ORBITER BENDING MODE

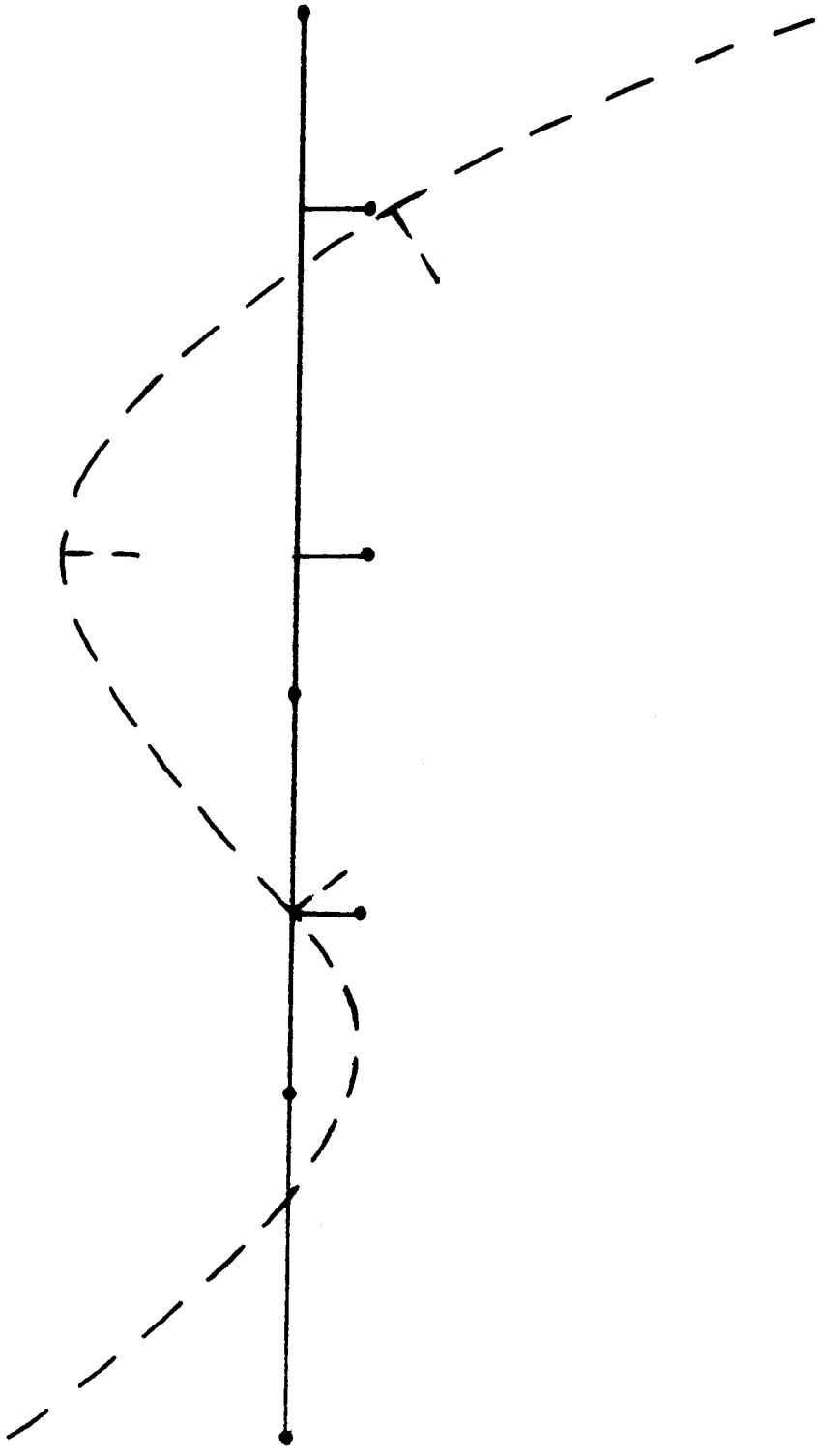

FIGURE 4 - SECOND ORBITER BENDING MODE

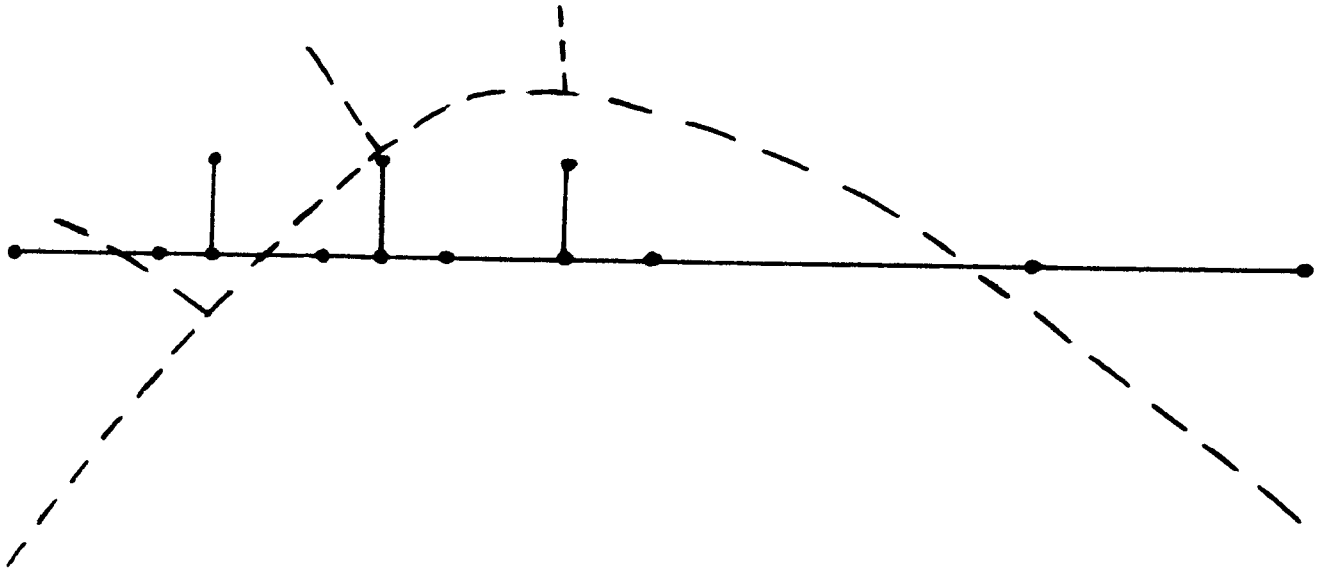

FIGURE 5 - FIRST FREE-FREE BOOSTER BENDING MODE

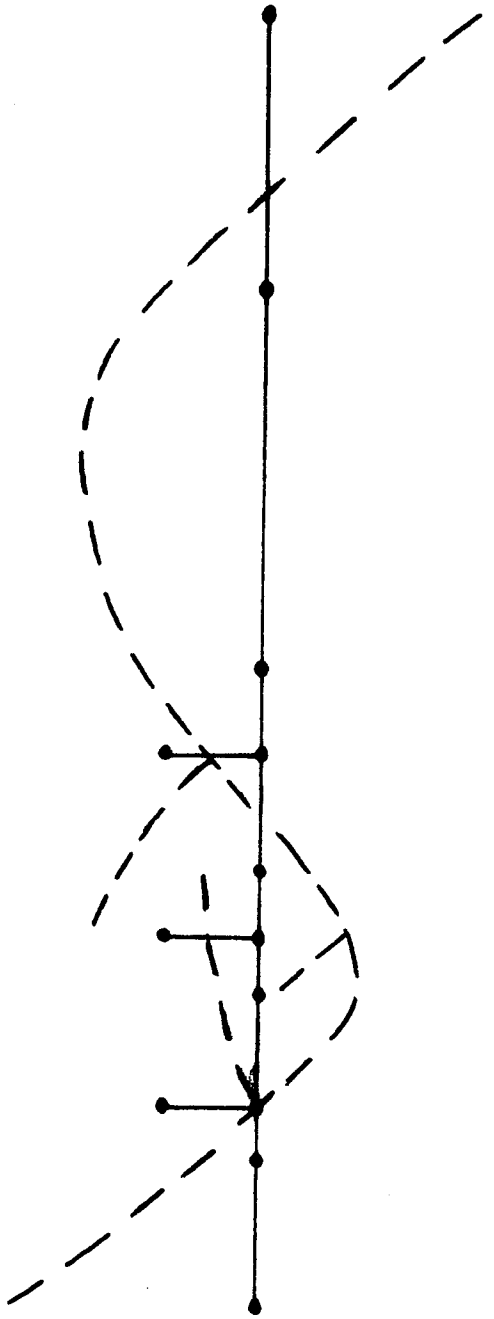

FIGURE 6 - SECOND FREE-FREE BOOSTER BENDING MODE

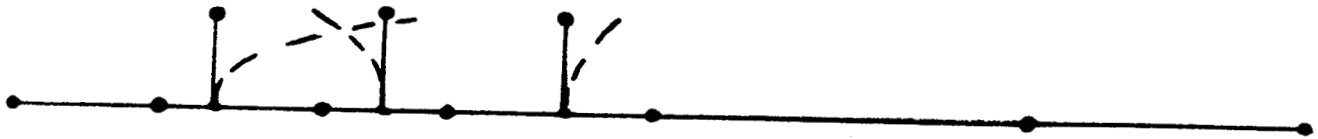

FIGURE 7 - FIRST FREE-FREE BOOSTER SPRING AXIAL MODE

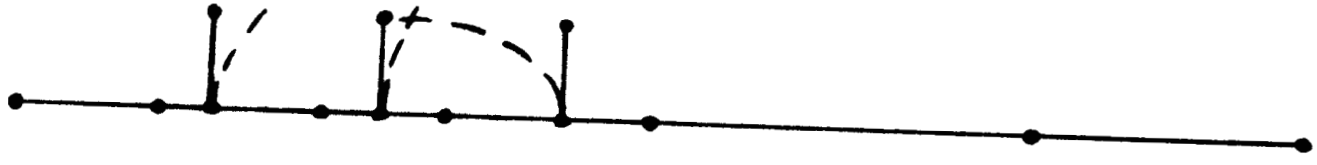

FIGURE 8 - SECOND FREE-FREE BOOSTER SPRING AXIAL MODE

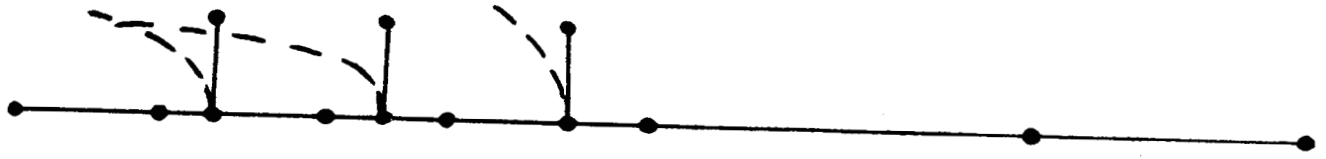

FIGURE 9 - THIRD FREE-FREE BOOSTER SPRING AXIAL MODE

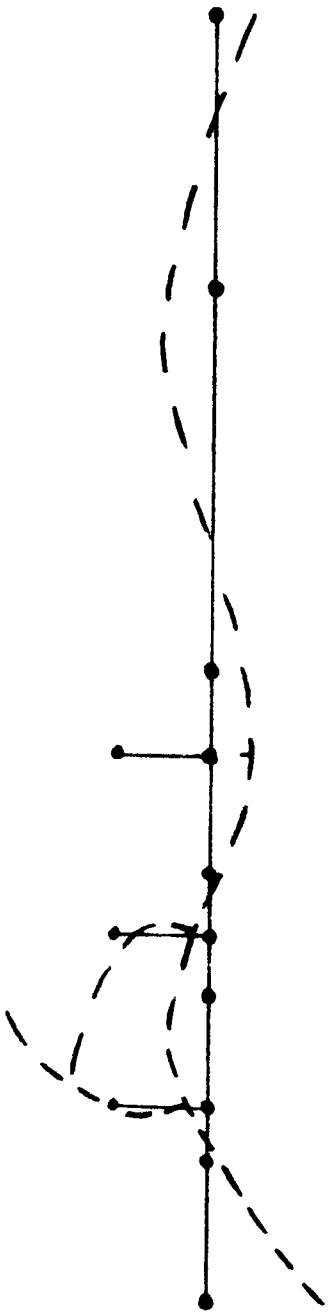

FIGURE 10 - THIRD FREE-FREE BOOSTER BENDING MODE

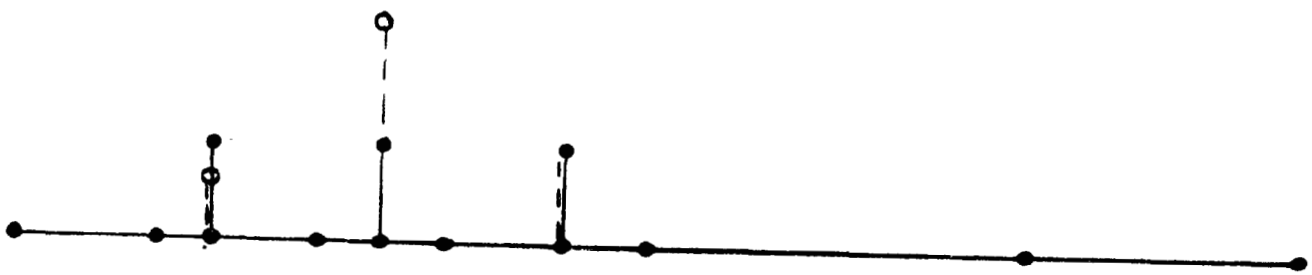

FIGURE 11 - FIRST FREE-FREE BOOSTER SPRING LATERAL MODE

FIGURE 12 - SECOND FREE-FREE BOOSTER SPRING LATERAL MODE

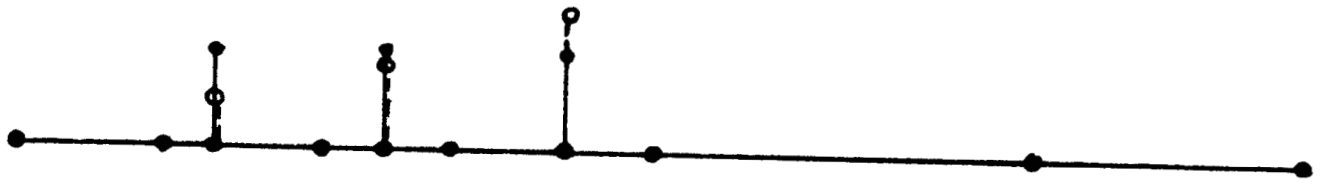

FIGURE 13 - THIRD FREE-FREE BOOSTER SPRING LATERAL MODE

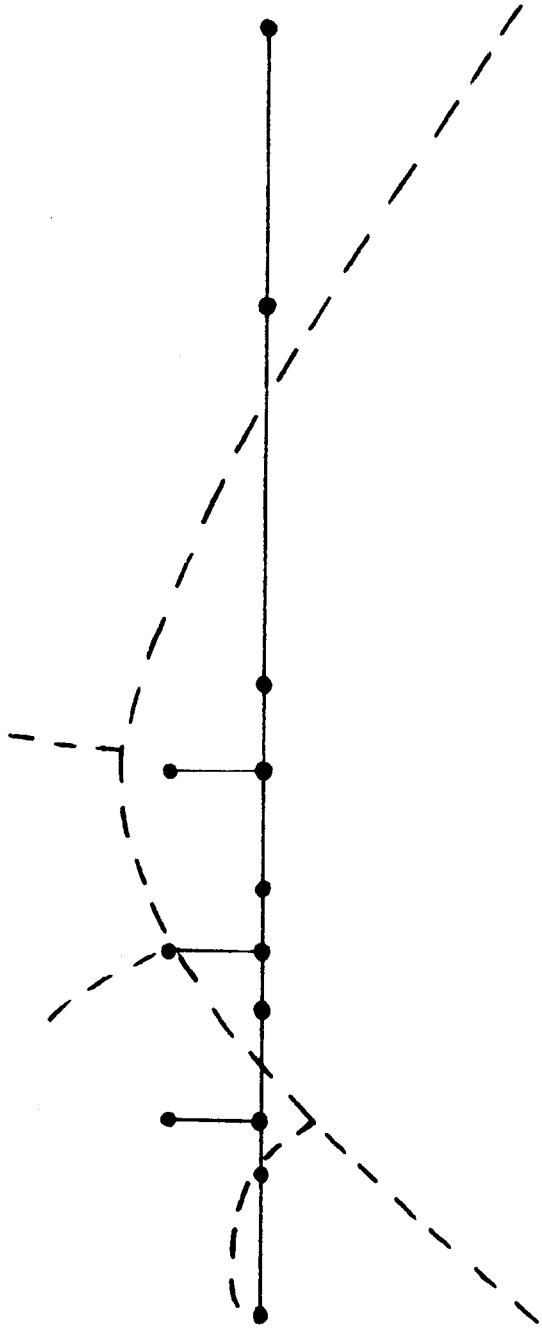

FIGURE 14 - FIRST MASS LOADED BOOSTER BENDING MODE

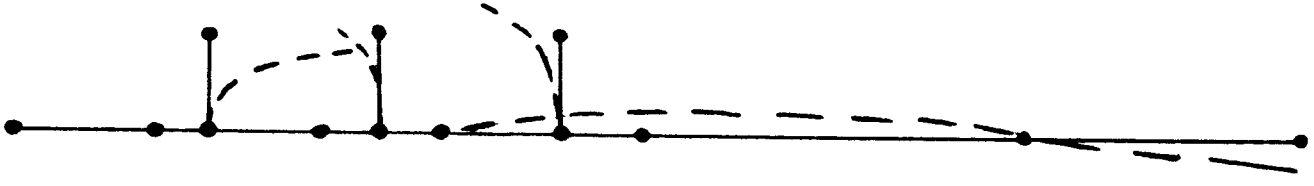

FIGURE 15 - FIRST MASS LOADED BOOSTER SPRING AXIAL MODE

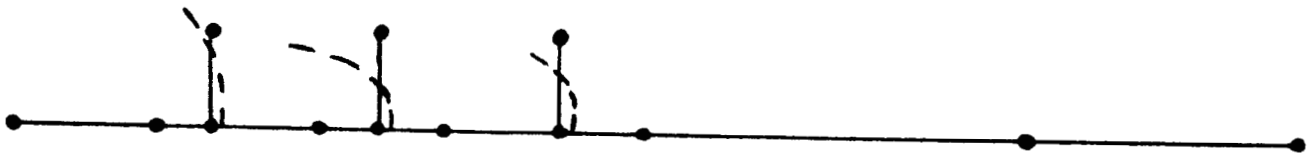

FIGURE 16 - THIRD MASS LOADED BOOSTER SPRING AXIAL MODE

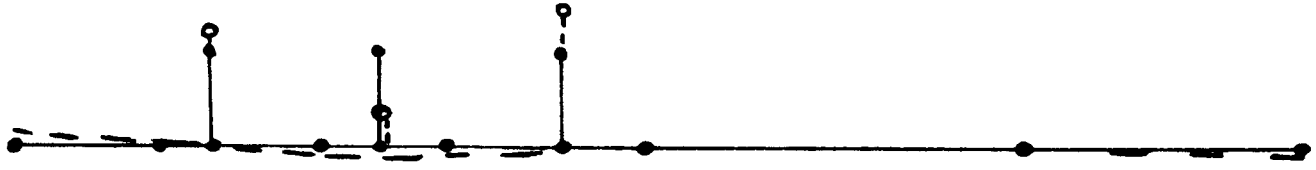

FIGURE 17 - FIRST MASS LOADED BOOSTER SPRING LATERAL MODE

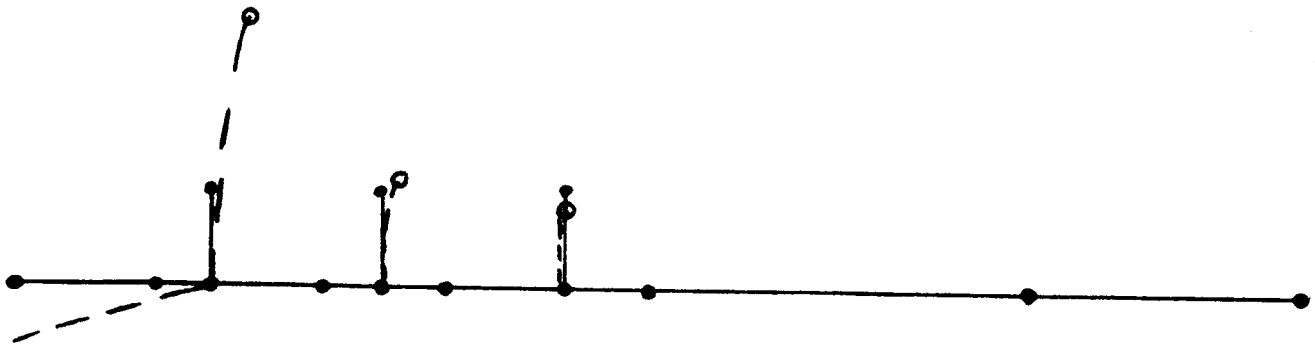

FIGURE 18 - SECOND MASS LOADED BOOSTER SPRING LATERAL MODE

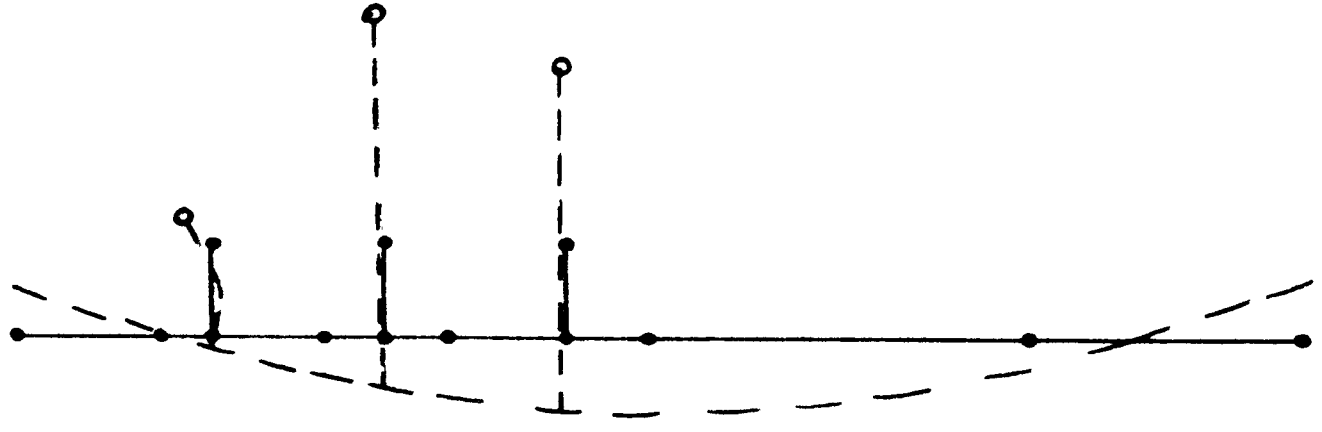

FIGURE 19 - THIRD MASS LOADED BOOSTER SPRING LATERAL MODE

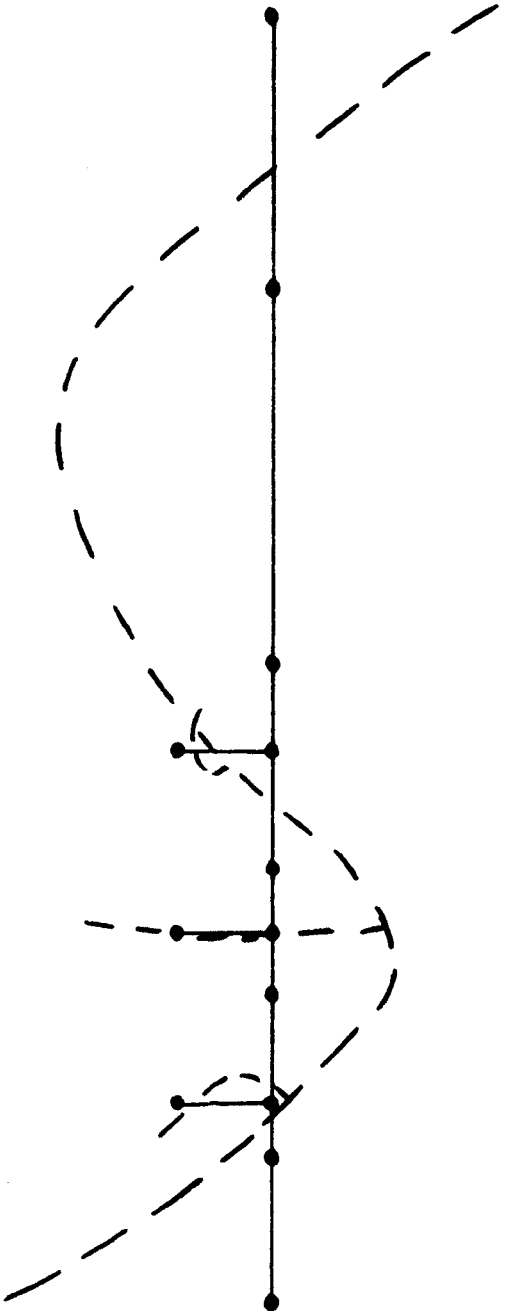

FIGURE 20 - SECOND MASS LOADED BOOSTER BENDING MODE

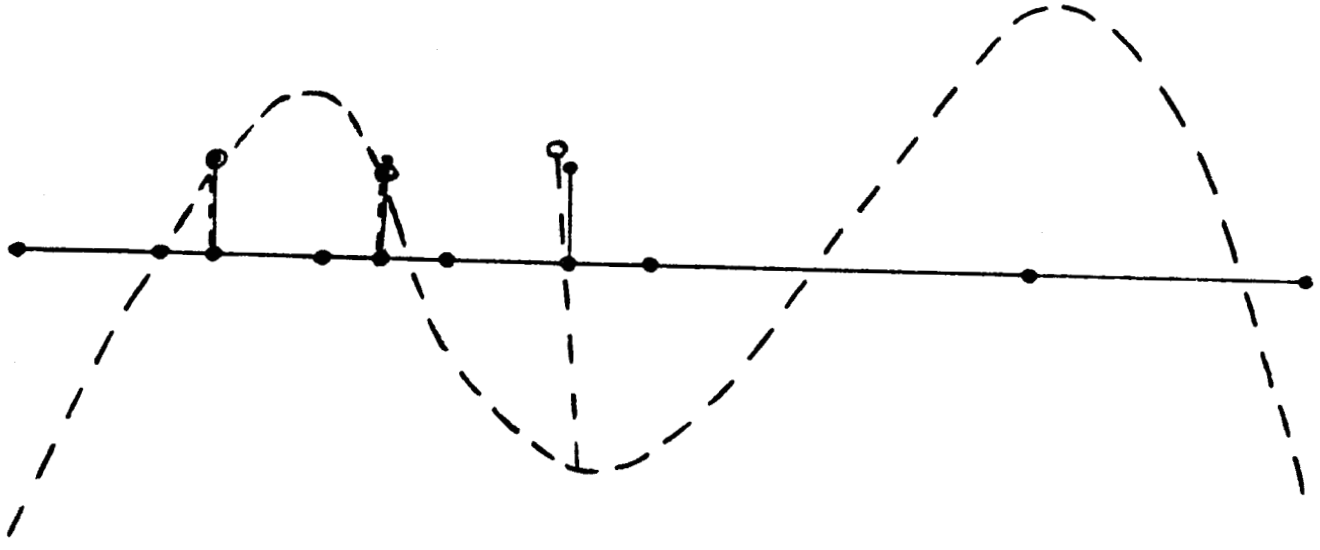

FIGURE 21 - THIRD MASS LOADED BOOSTER BENDING MODE

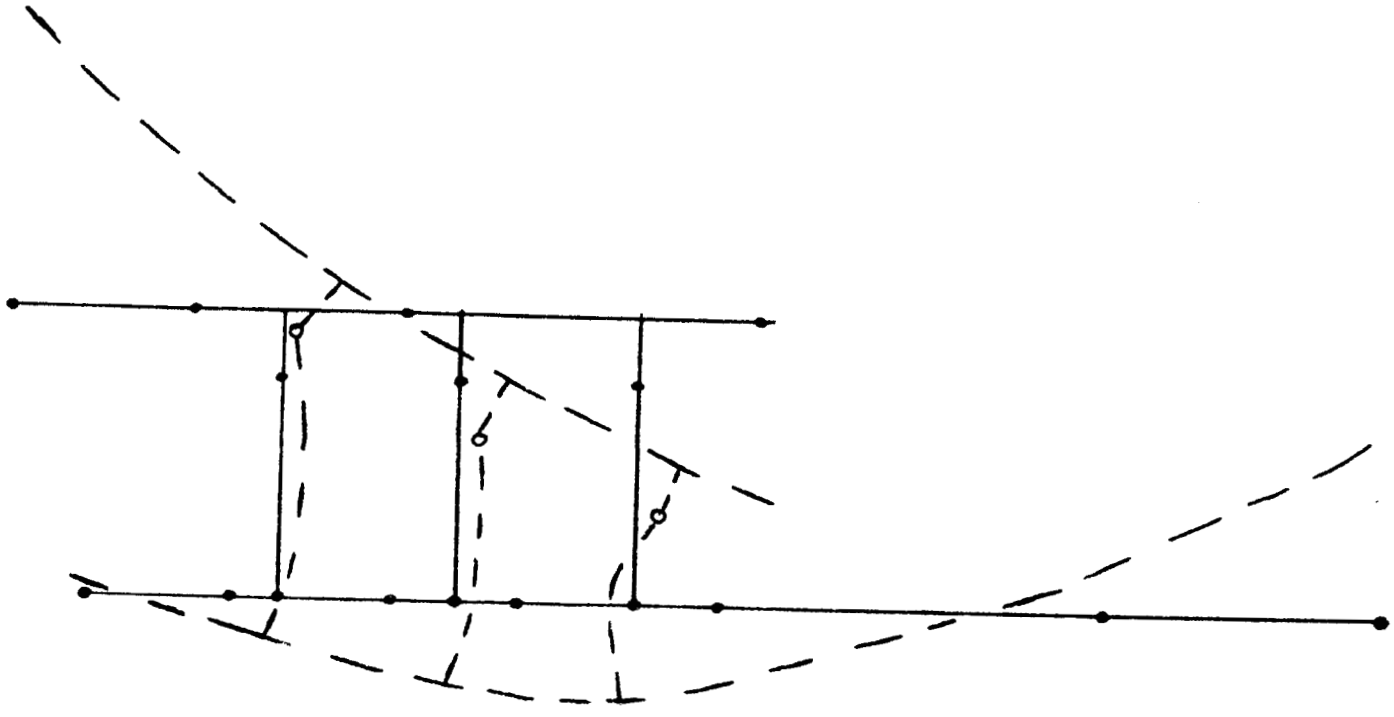

FIGURE 22 - FIRST ORBITER / BOOSTER MODE (ANALYSIS)

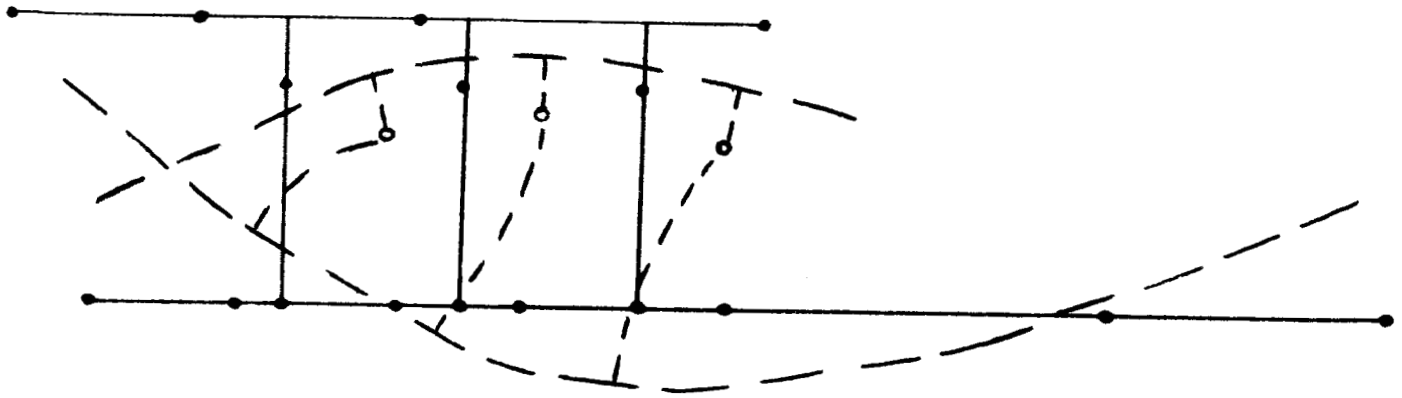

FIGURE 23 - SECOND ORBITER / BOOSTER MODE (ANALYSIS)

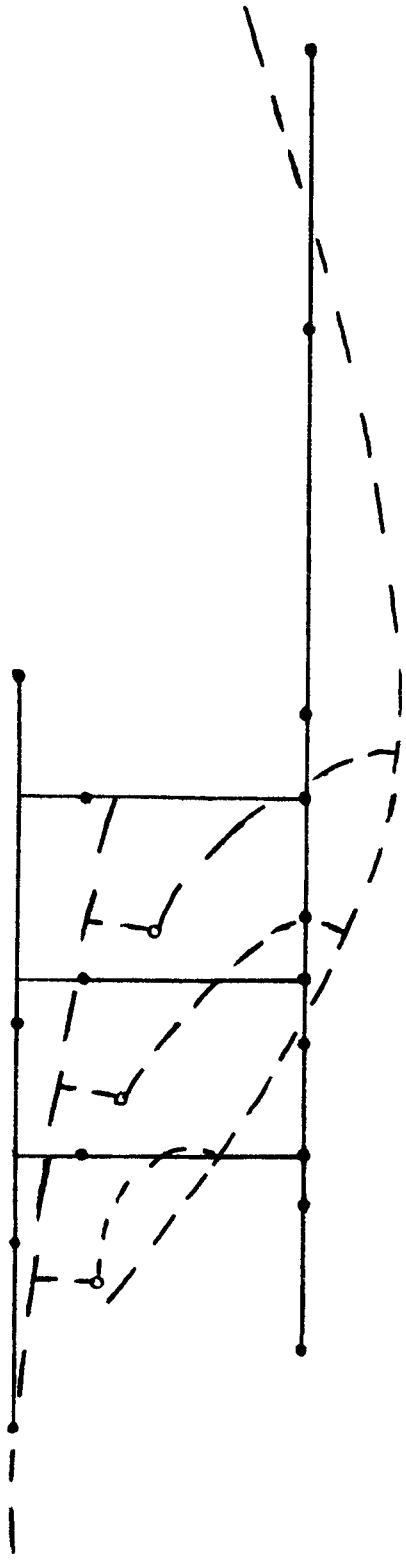

FIGURE 24 - THIRD ORBITER / BOOSTER MODE (ANALYSIS)

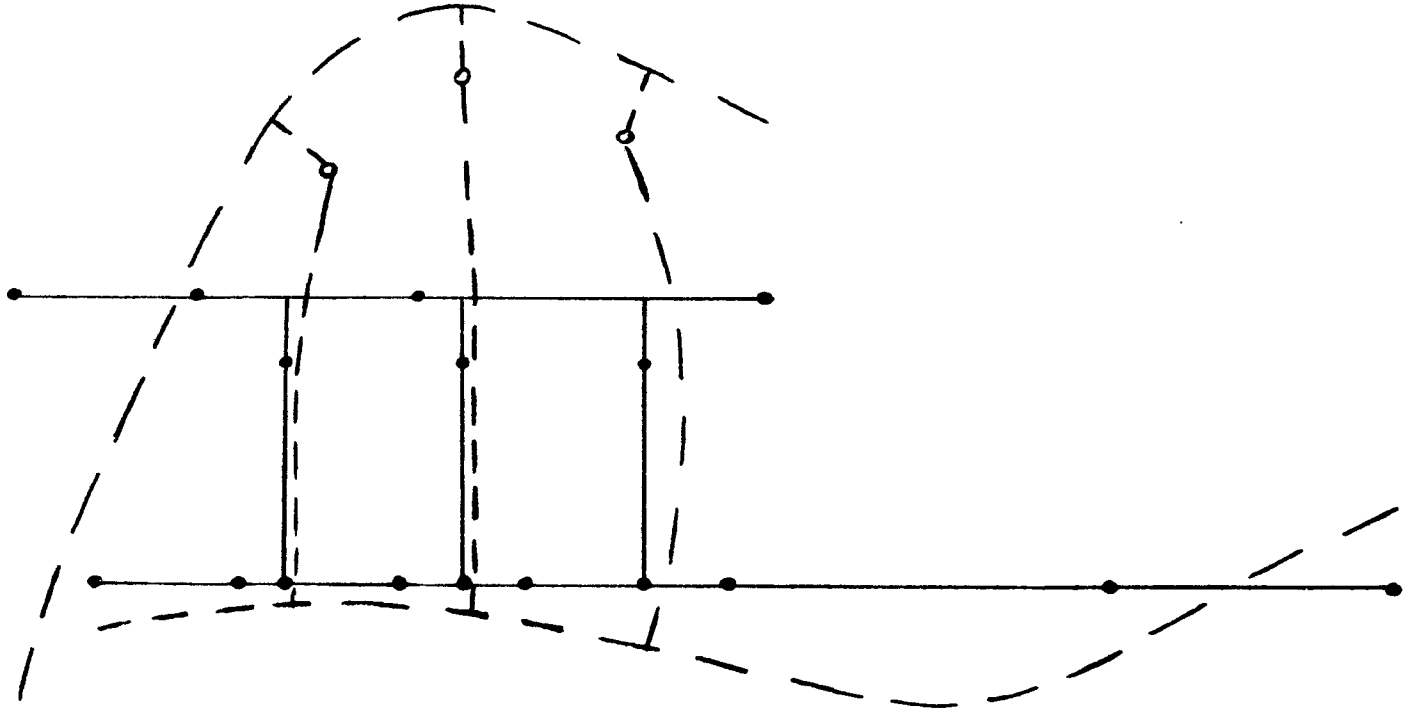

FIGURE 25 - FOURTH ORBITER / BOOSTER MODE (ANALYSIS)

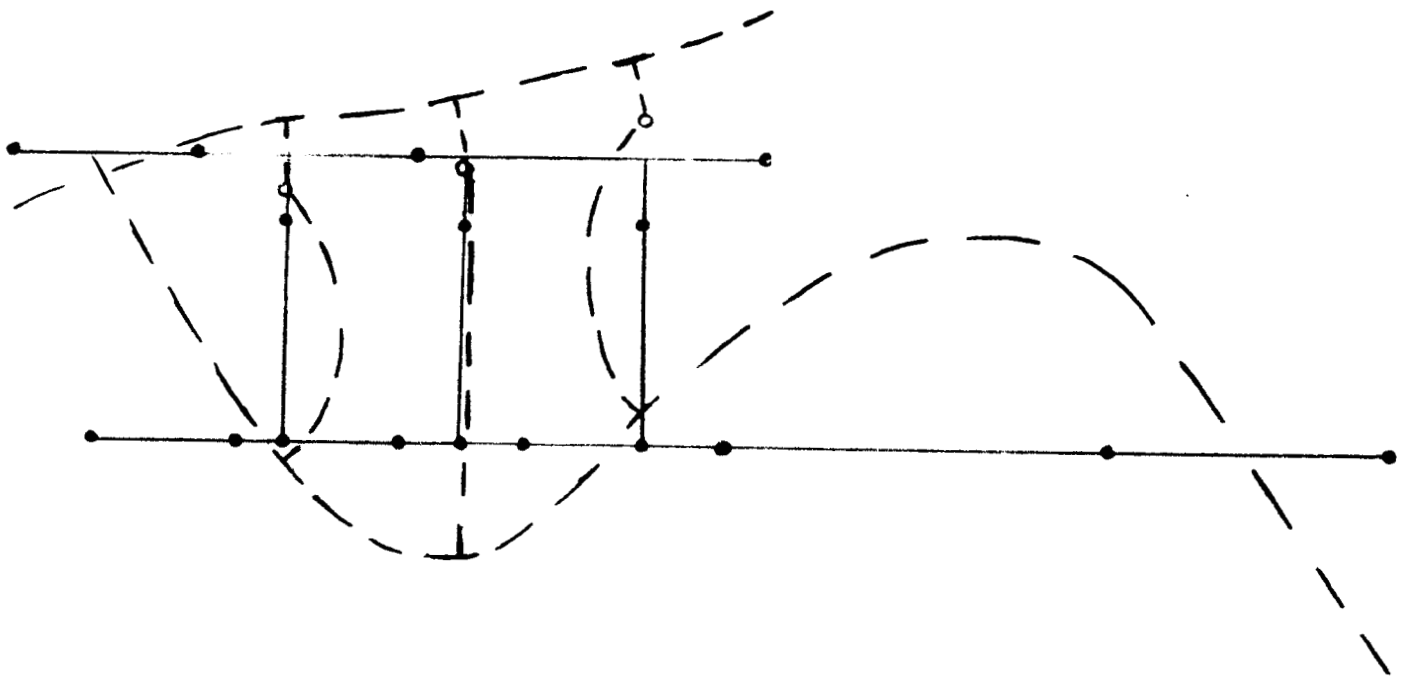

FIGURE 26 - FIFTH ORBITER/BOOSTER MODE (ANALYSIS)

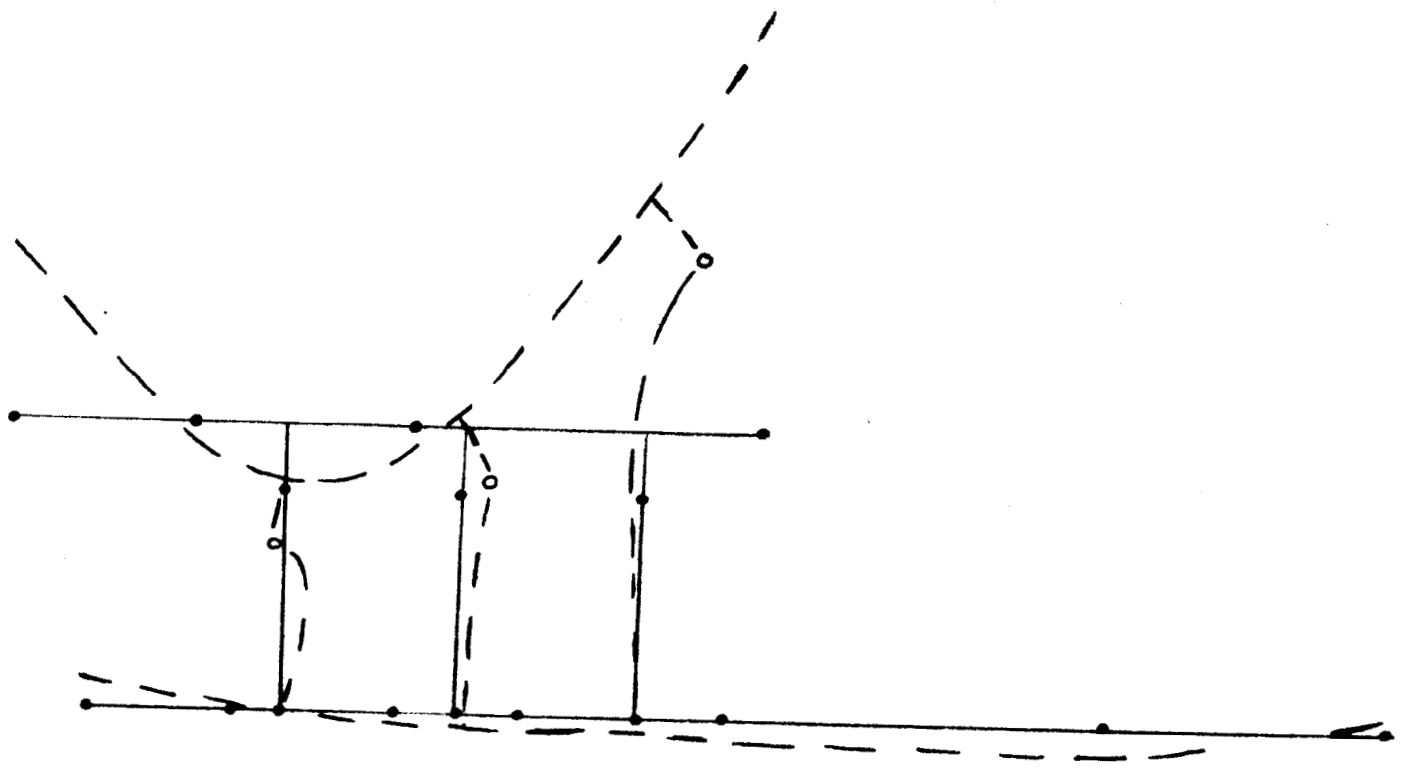

FIGURE 27 - SIXTH ORBITER / BOOSTER MODE (ANALYSIS)

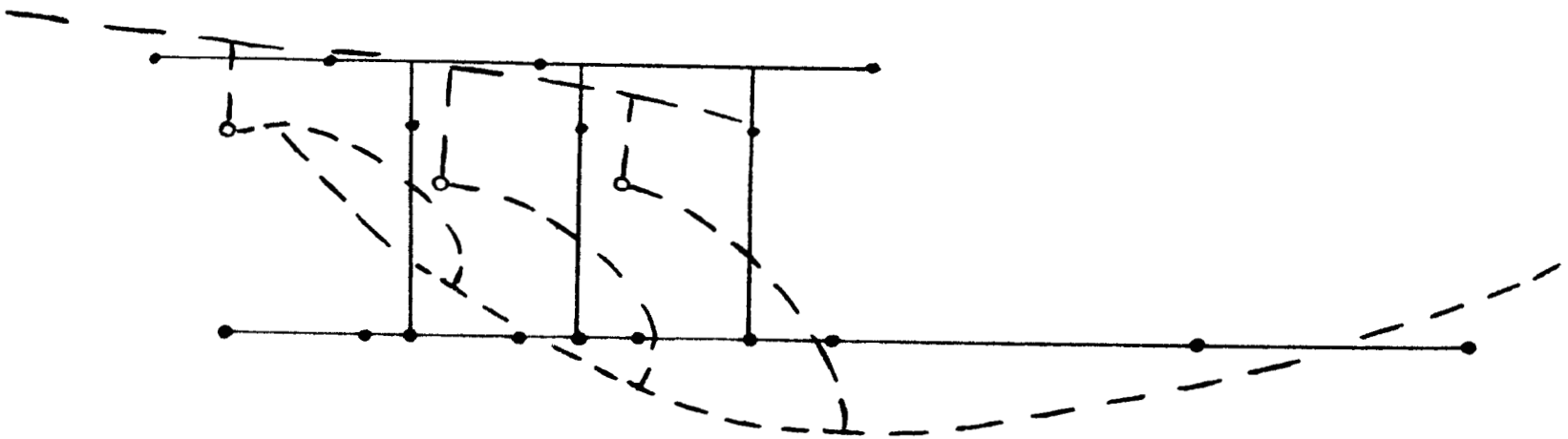

FIGURE 28 - THIRD ORBITER / BOOSTER MODE (TEST)

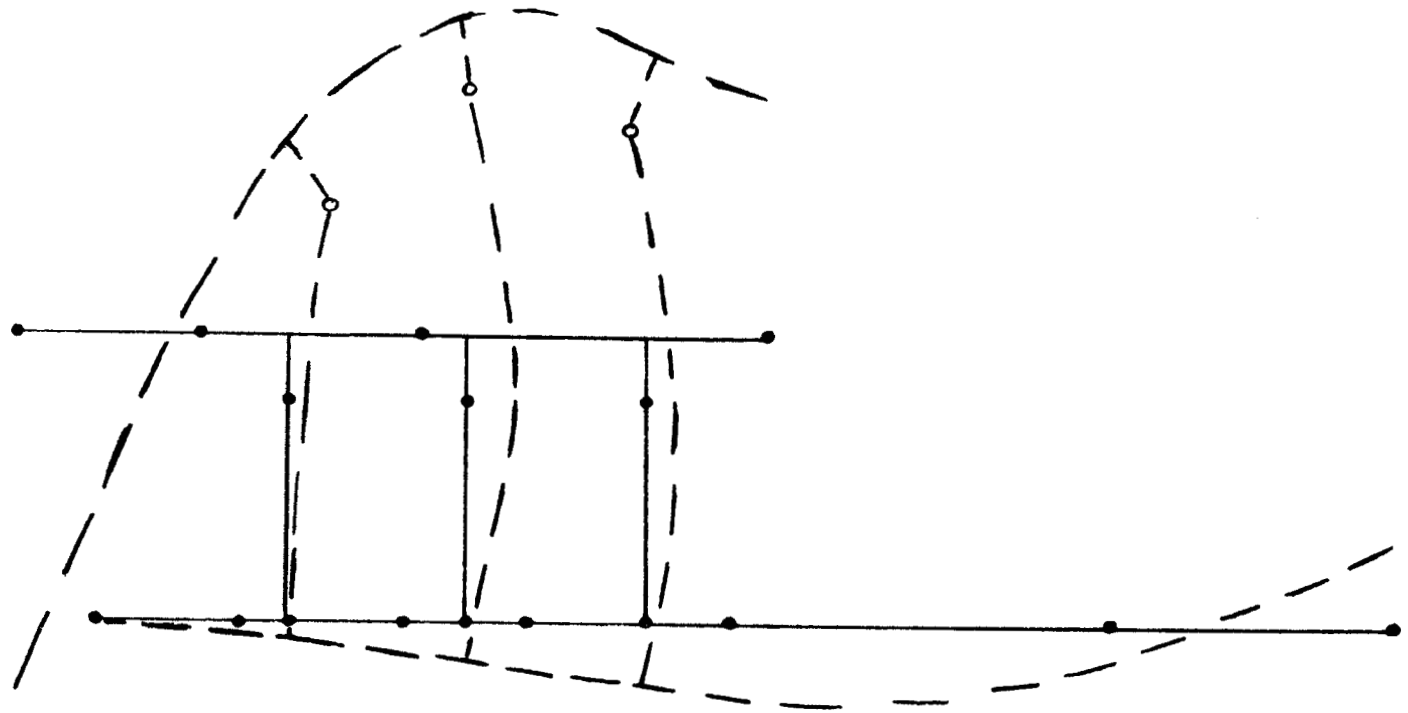

FIGURE 29 - FOURTH ORBITER / BOOSTER MODE (TEST)

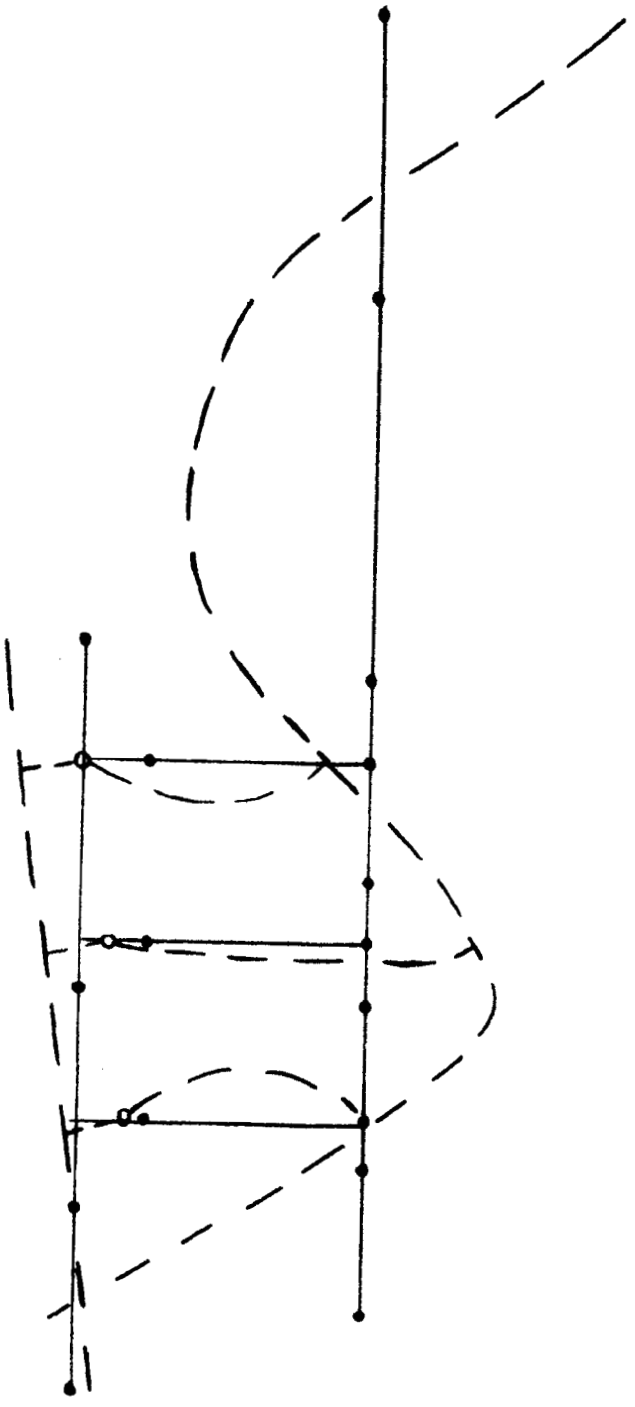

FIGURE 30 - FIFTH ORBITER / BOOSTER MODE (TEST)

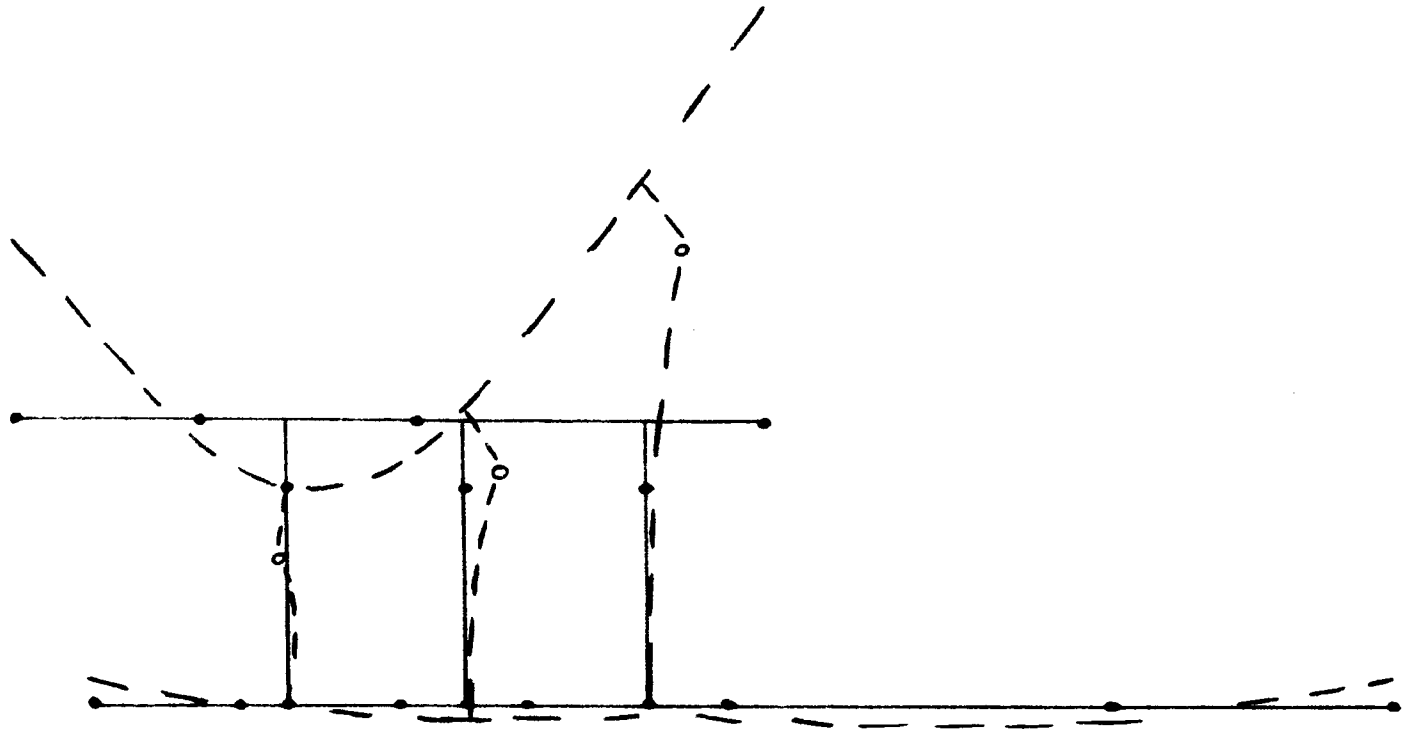

FIGURE 31 - SIXTH ORBITER / BOOSTER MODE (TEST)

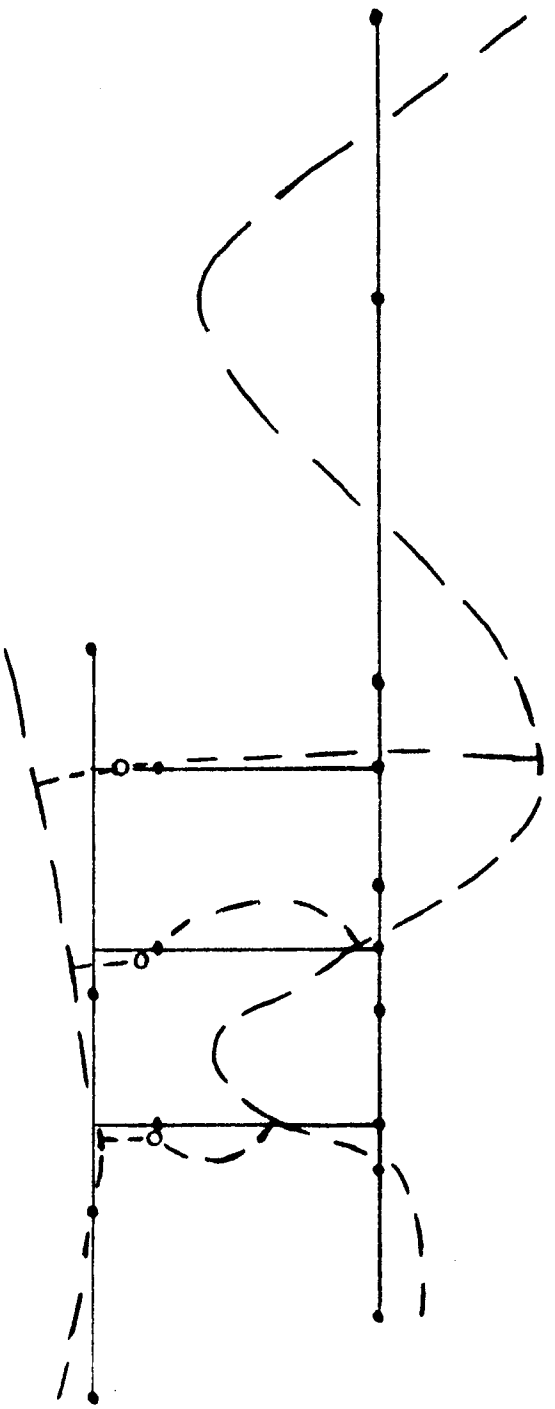

FIGURE 32 - SEVENTH ORBITER / BOOSTER MODE (TEST)

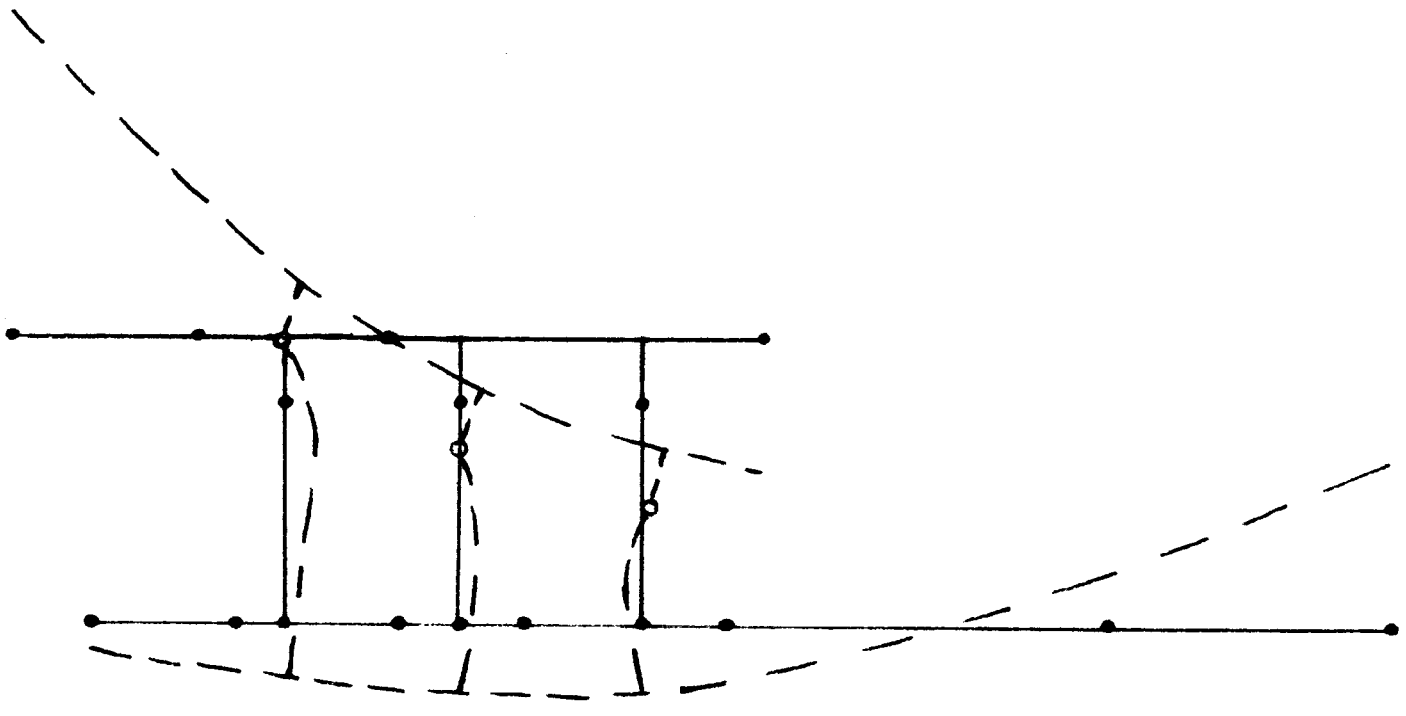

FIGURE 33 - FIRST ORBITER / BOOSTER MODE (FREE - FREE SYNTHESIS)

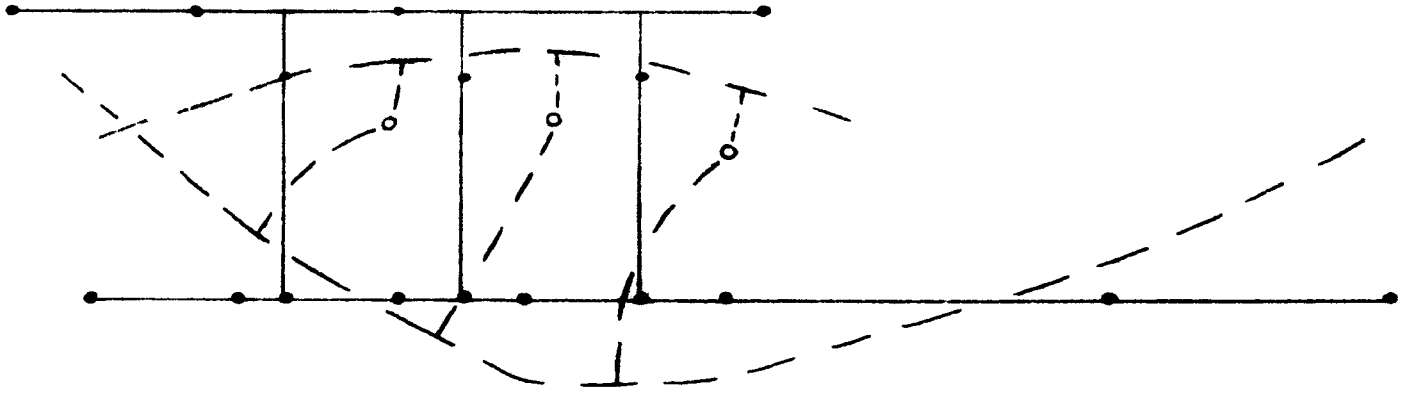

FIGURE 34 - SECOND ORBITER / BOOSTER MODE (FREE - FREE SYNTHESIS)

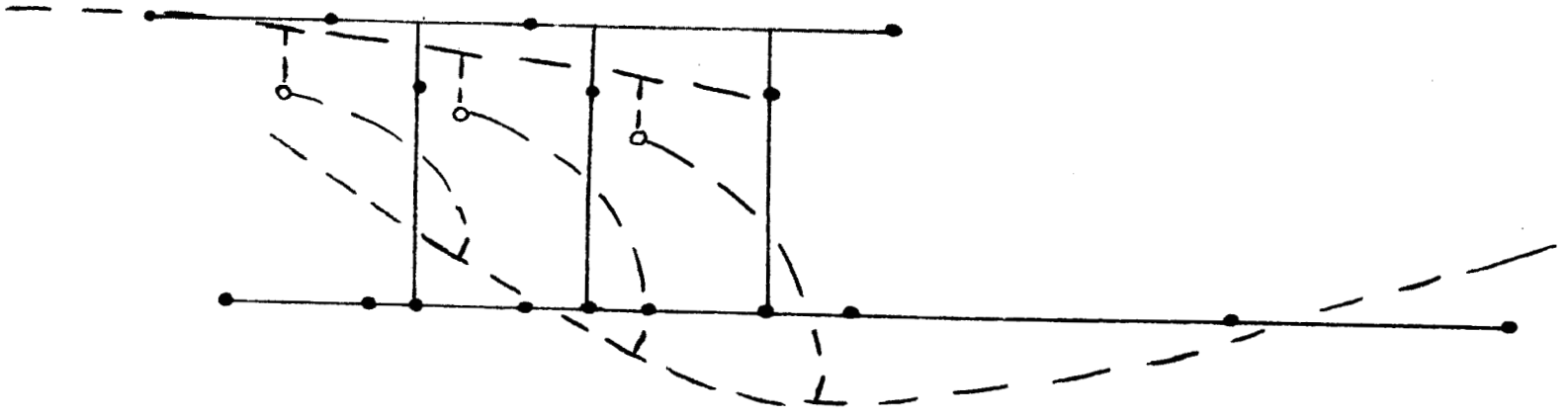

FIGURE 35 - THIRD ORBITER / BOOSTER MODE (FREE - FREE SYNTHESIS)

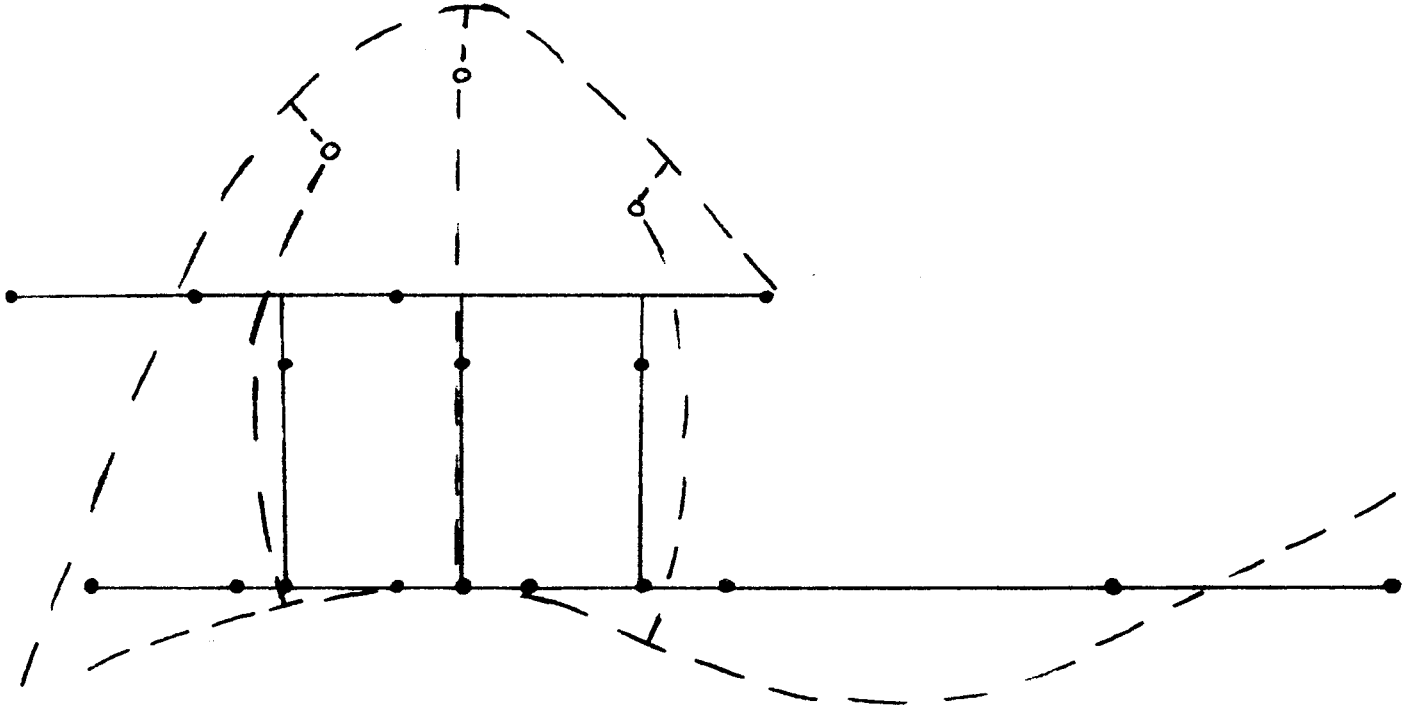

FIGURE 36 - FOURTH ORBITER / BOOSTER MODE (FREE - FREE SYNTHESIS)

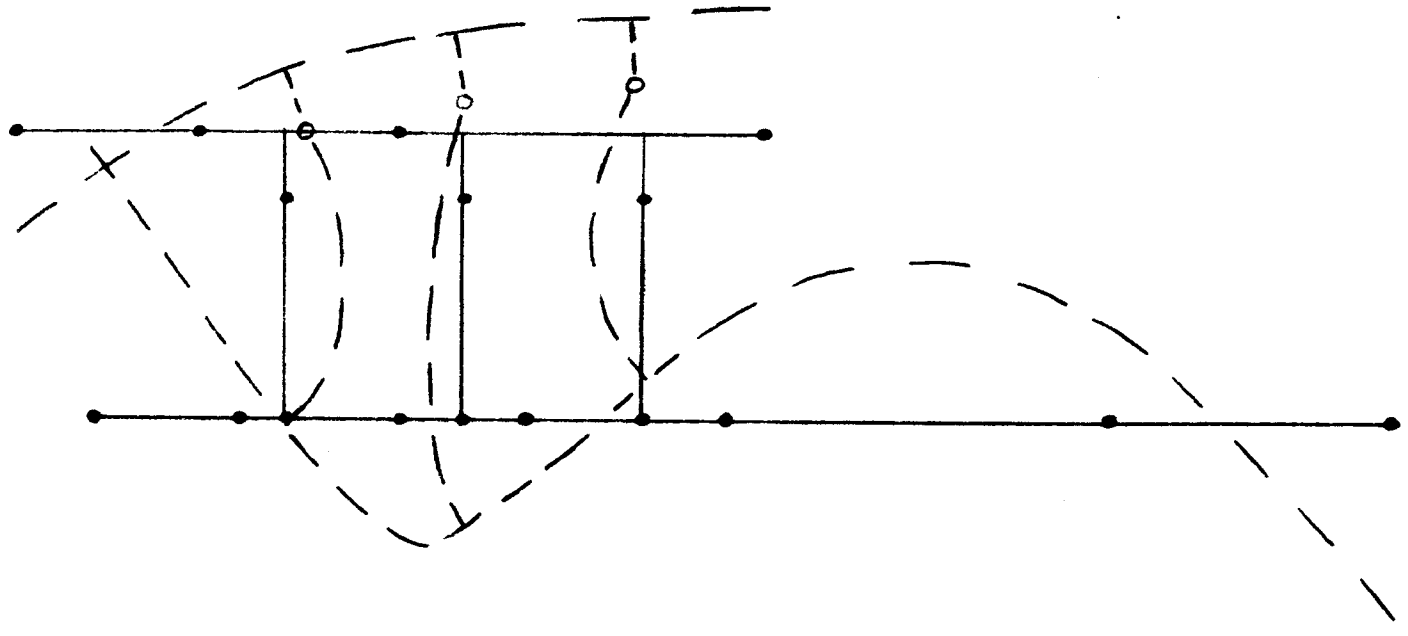

FIGURE 37 - FIFTH ORBITER / BOOSTER MODE (FREE - FREE SYNTHESIS)

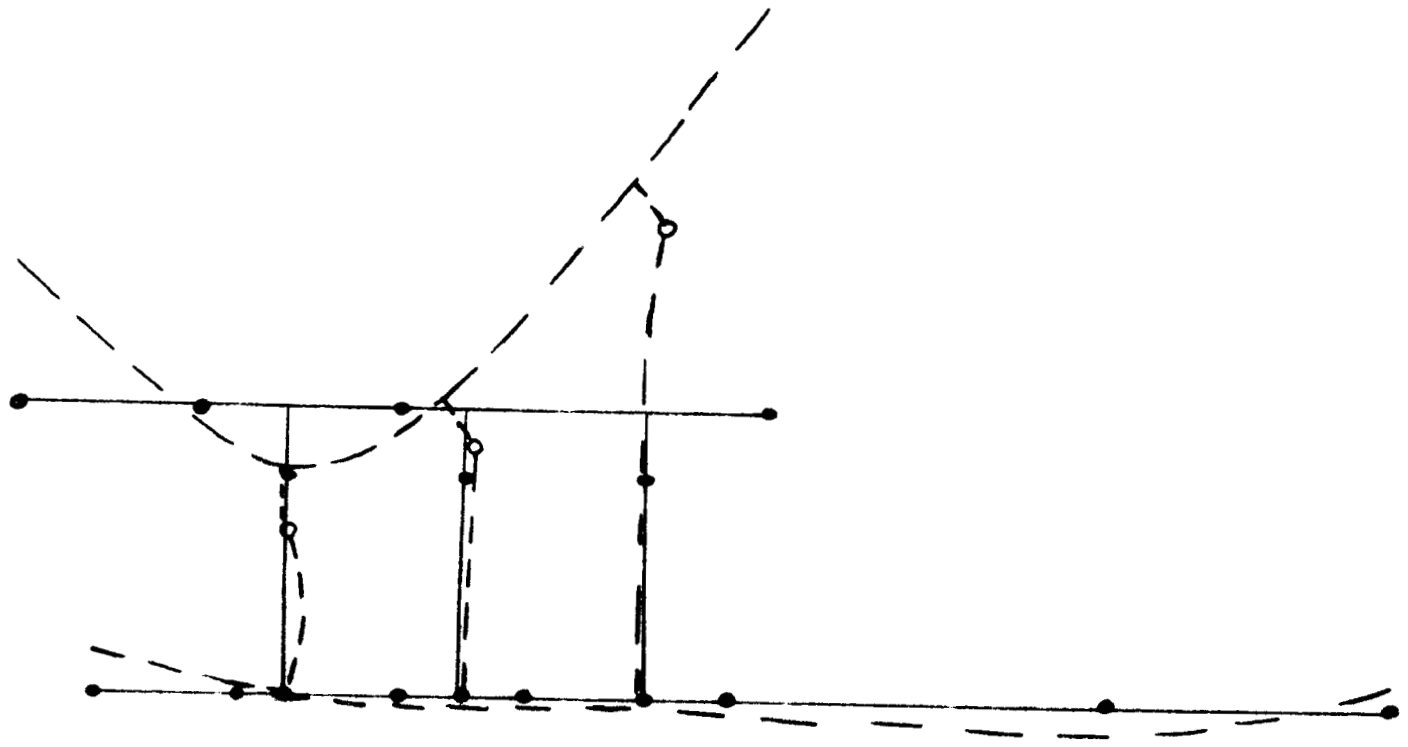

FIGURE 38 - SIXTH ORBITER / BOOSTER MODE (FREE - FREE SYNTHESIS)

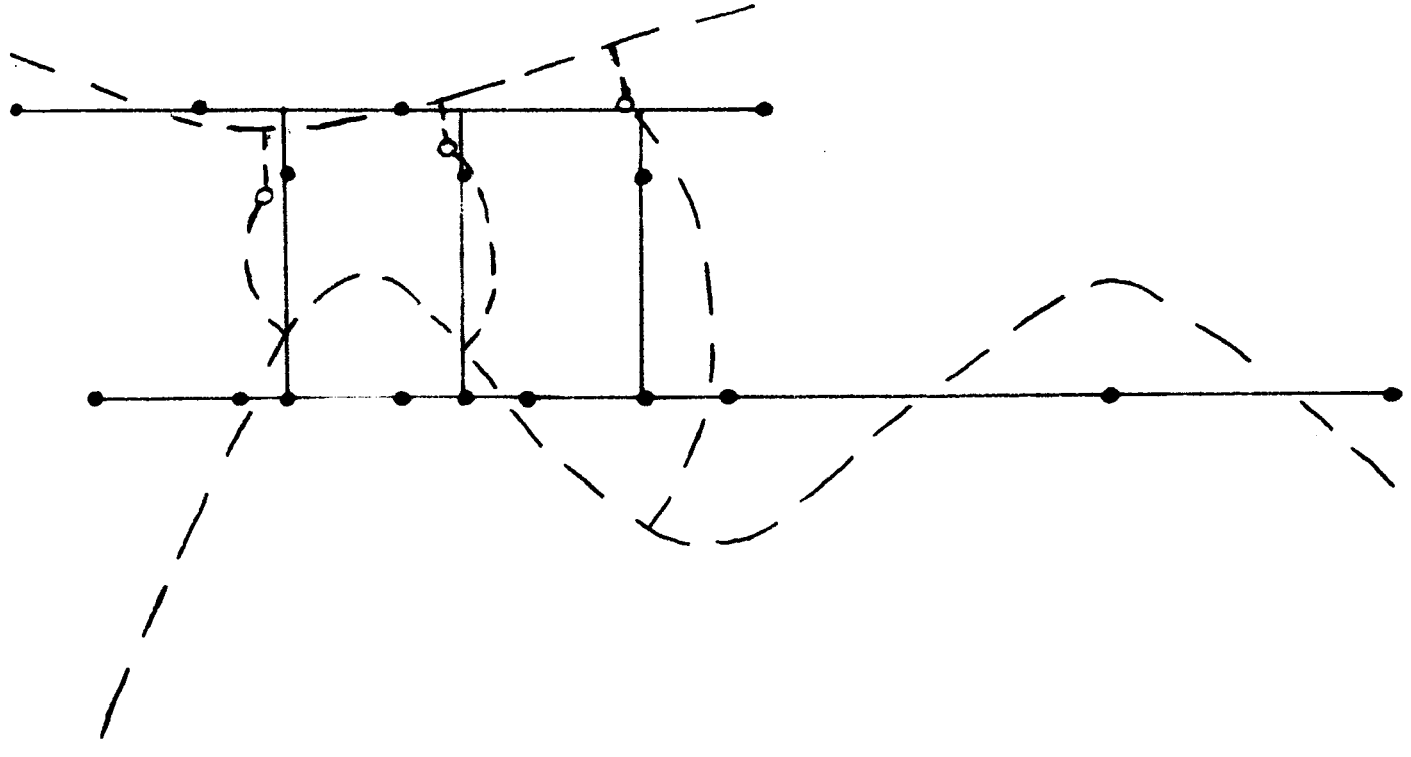

FIGURE 39 - SEVENTH ORBITER / BOOSTER MODE (FREE - FREE SYNTHESIS)

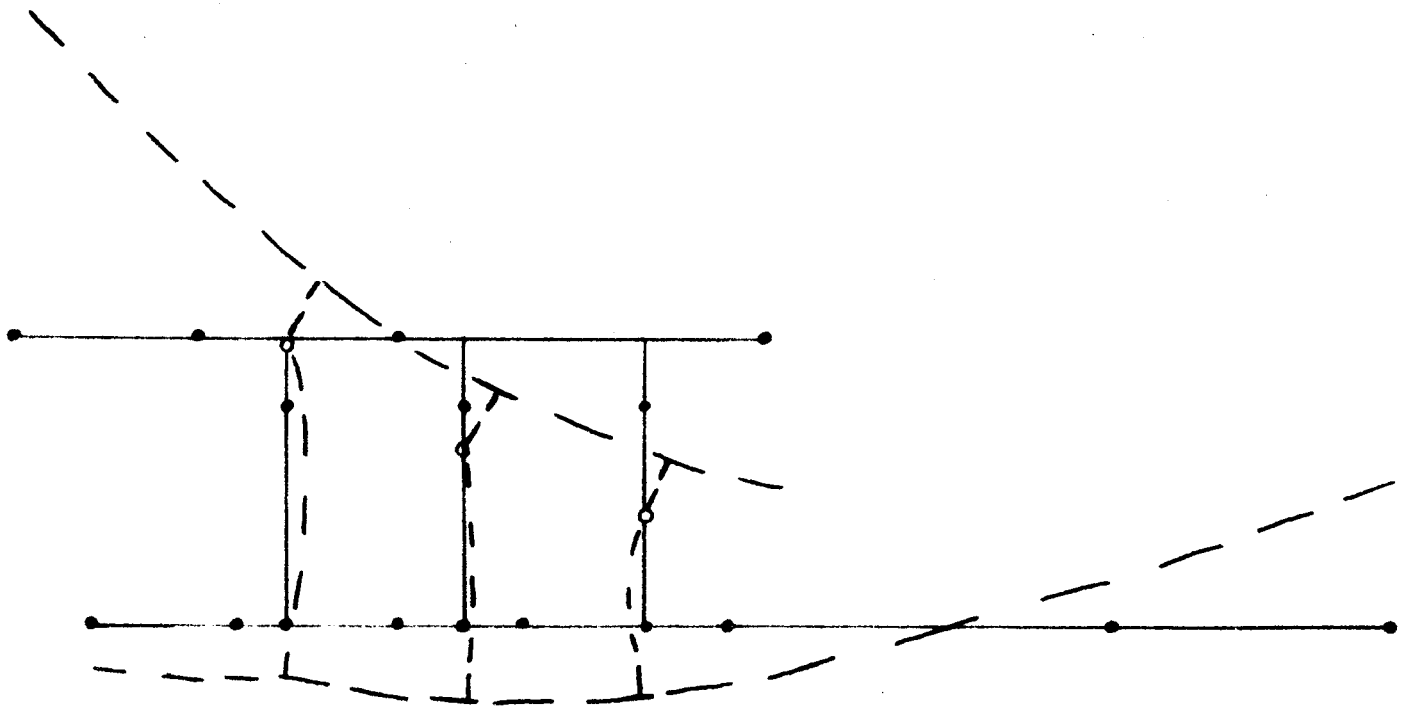

FIGURE 40 - FIRST ORBITER / BOOSTER MODE (MASS LOADED SYNTHESIS)

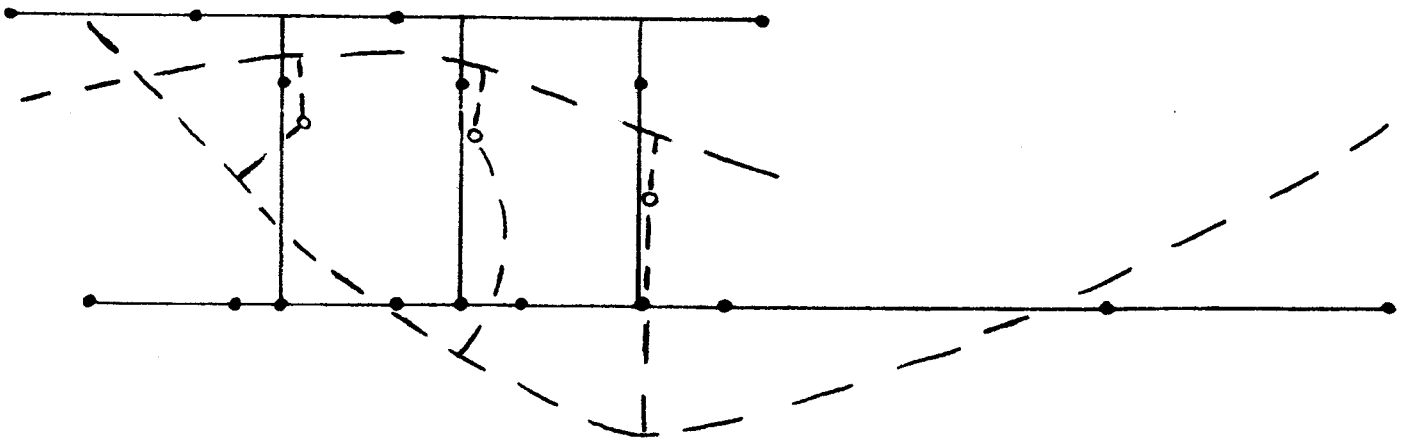

FIGURE 41 - SECOND ORBITER / BOOSTER MODE (MASS LOADED SYNTHESIS)

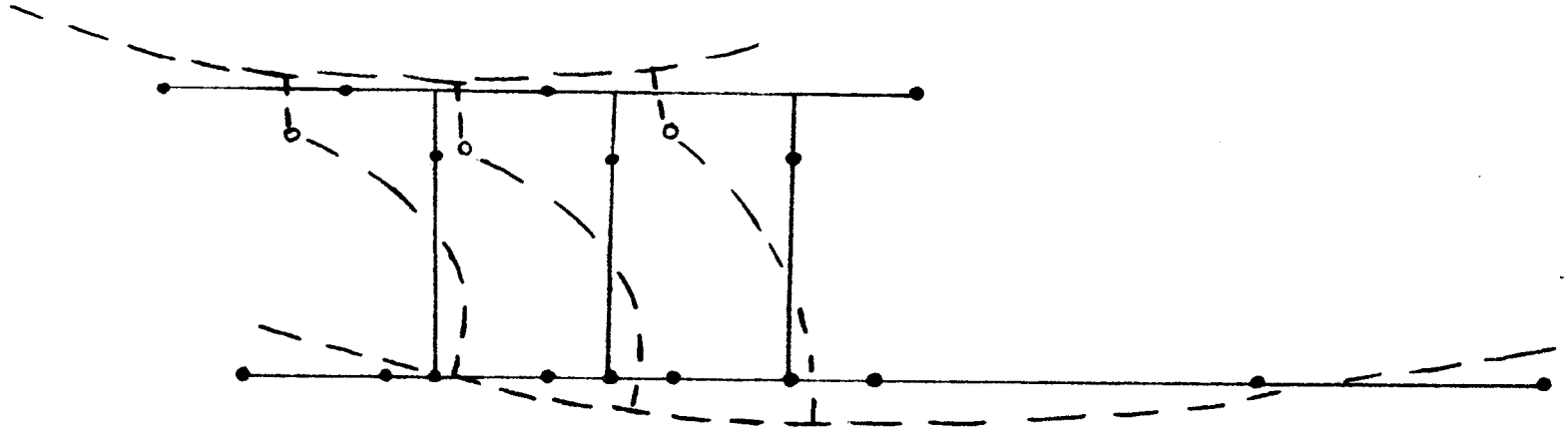

FIGURE 42 - THIRD ORBITER / BOOSTER MODE (MASS LOADED SYNTHESIS)

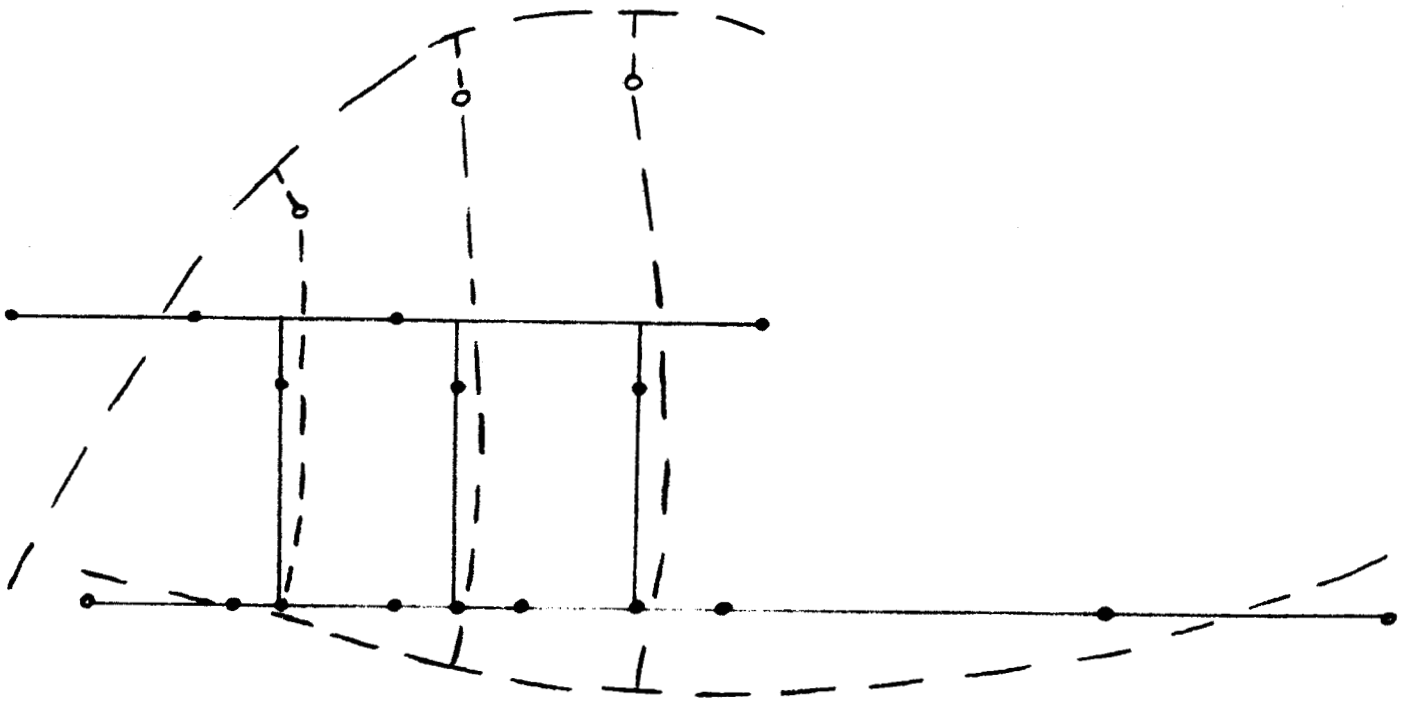

FIGURE 43 - FOURTH ORBITER / BOOSTER MODE (MASS LOADED SYNTHESIS)

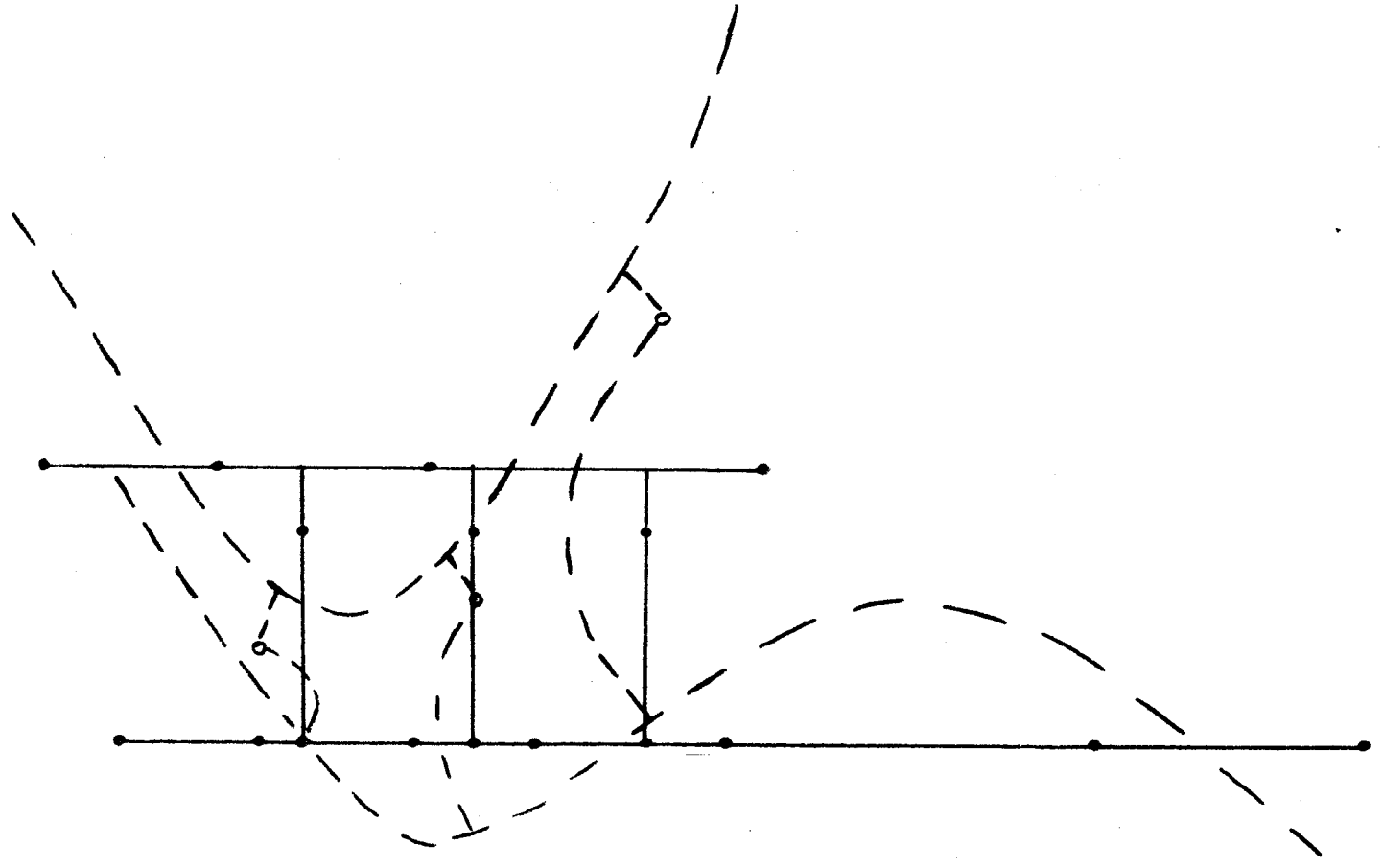

FIGURE 44 - FIFTH ORBITER / BOOSTER MODE (MASS LOADED SYNTHESIS)

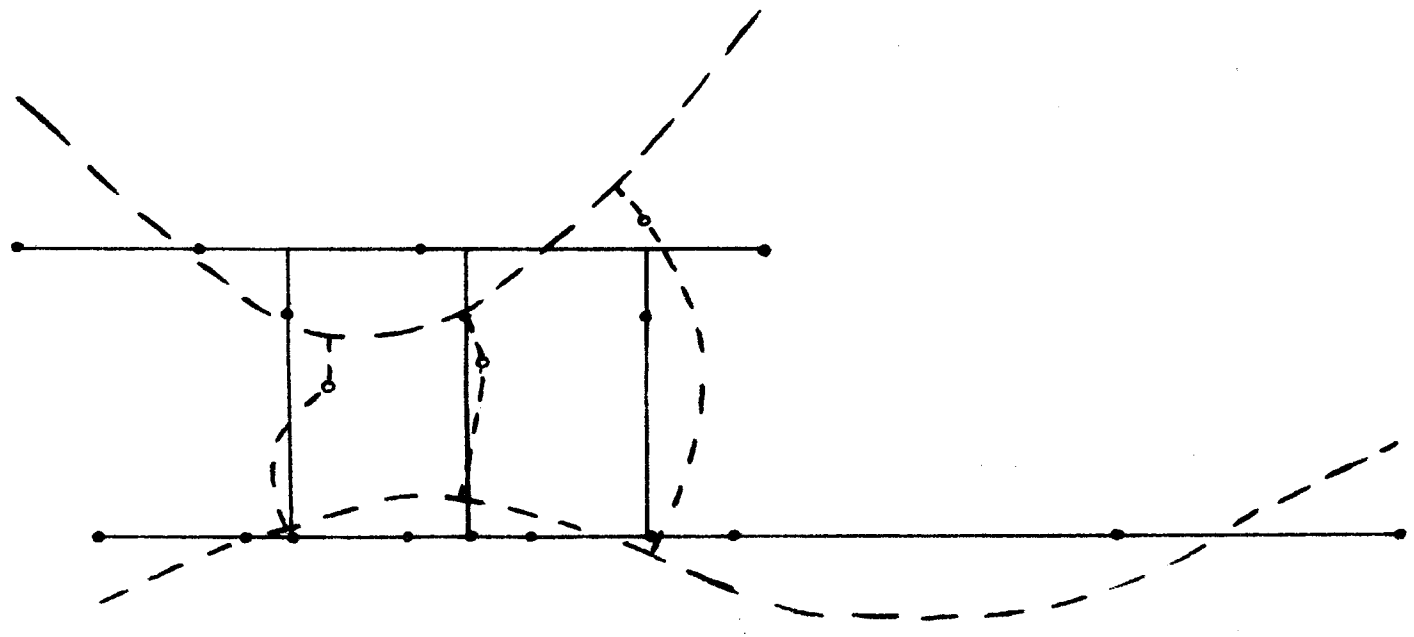

FIGURE 45 - SIXTH ORBITER / BOOSTER MODE (MASS LOADED SYNTHESIS)

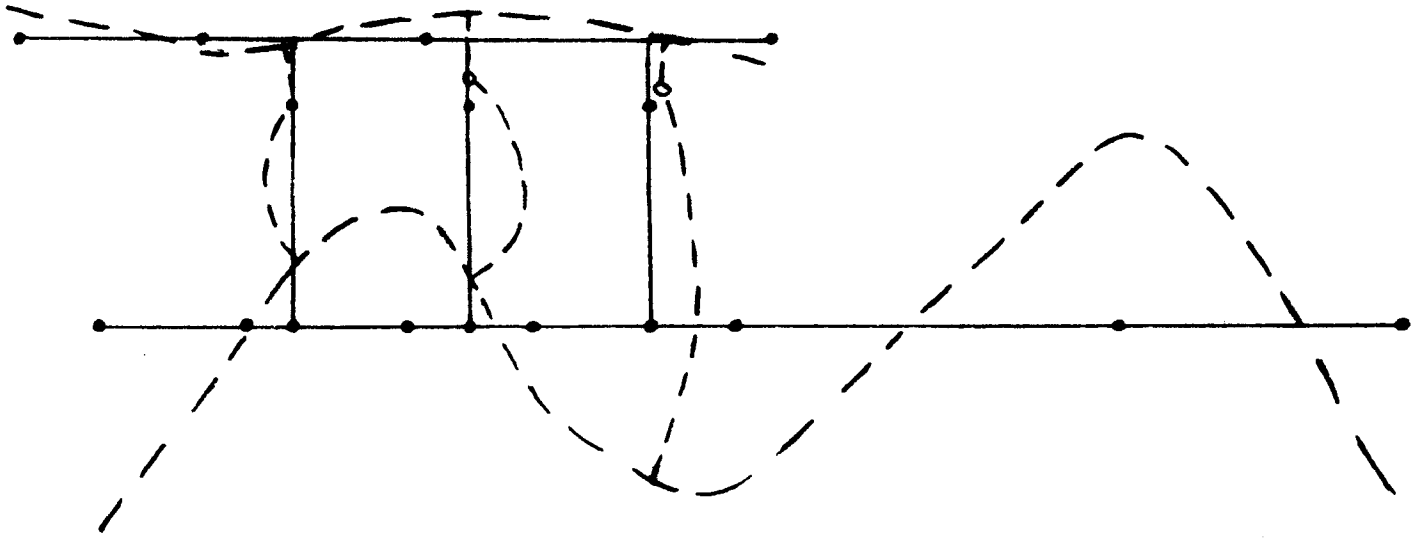

FIGURE 46 - SEVENTH ORBITER / BOOSTER MODE (MASS LOADED SYNTHESIS)